METAMORPHIC EVOLUTION OF METAPELITES IN THE HIGH-PRESSURE TERRANE OF THE RHODOPE ZONE, NORTHERN GREECE

EVRIPIDIS MPOSKOS AND ANTHI LIATI

*Section of Geological Sciences, National Technical University of Athens,
Iroon Polytechniou 9, 15773 Zografou, Athens, Greece*

ABSTRACT

The Rhodope zone of northern Greece has been involved in an Alpine metamorphic cycle that consists of a high-pressure (eclogite-facies) metamorphism extensively overprinted under medium-pressure conditions in Eocene time. Abrupt differences in the grade of metamorphism within the Rhodope zone allows its subdivision into a lower and an upper tectonic unit. The pelitic rocks of the lower tectonic unit are typically garnet – chloritoid ± staurolite schists. These rocks preserve the high-pressure paragenesis garnet + chloritoid + chlorite + phengite + quartz + rutile. Minerals formed during exhumation are staurolite, muscovite, Fe-rich chlorite and, rarely, biotite and andalusite. In the upper tectonic unit, the metapelites are generally garnet – biotite ± kyanite gneisses and schists; the high-pressure paragenesis has been partly obliterated during extensive retrograde overprinting. Peak (minimum) conditions of pressure determined for the lower tectonic unit by use of the phengite geobarometer (for T = 550° to 600°C) are 13–13.5 kbar. P–T estimates for peak of metamorphism of the upper tectonic unit are uncertain. Textural features and mineral chemical data provide information on metamorphic conditions for various stages of decompression of both units. The exhumation path of the lower tectonic unit was nearly isothermal to a depth of ~12 km from the surface. In the upper tectonic unit, exhumation proceeded along a P–T path characterized by cooling. These differences are probably attributed to thrusting of the deeper lying, upper tectonic unit over the lower one at depth during unloading. In this case, the upper unit acted as a warm "shield" and prevented the rocks of the underlying lower unit from losing heat. Since the P–T path of Rhodope shows important similarities in form with that of other high-pressure terranes (*i.e.*, the Western Alps, the Seward Peninsula in Alaska, the Cyclades in the Aegean Sea), analogous constraints, such as rapid unroofing tectonics or continuous underthrusting of cold material, can be invoked to explain the cooling that accompanied exhumation.

Keywords: metapelites, high-pressure metamorphism, eclogite-facies metamorphism, Rhodope zone, Greece.

SOMMAIRE

La zone de Rhodope, dans le nord de la Grèce, a été impliquée dans le cycle métamorphique Alpin, et a subi un métamorphisme à haute pression (faciès éclogite), qui a par la suite, durant l'Éocène, été remanié sous conditions de pressions moyennes. Des différences abruptes dans le degré du métamorphisme à l'intérieur de la zone de Rhodope permettent une subdivision en unités tectoniques inférieure et supérieure. Les roches pélitiques de l'unité inférieure sont typiquement transformées en schistes à grenat + chloritoïde ± staurotide. Ces roches conservent la paragenèse à pression élevée: grenat + chloritoïde + chlorite + phengite + quartz + rutile. Les minéraux formés lors de l'exhumation sont staurotide, muscovite, chlorite ferrifère et, moins couramment, biotite et andalousite. Dans l'unité tectonique supérieure, les métapélites sont en général des schistes et des gneiss à grenat + biotite ± kyanite. La paragenèse à pression élevée a partiellement été oblitérée au cours d'un métamorphisme rétrograde répandu. La pression maximale du métamorphisme, déterminée pour l'unité inférieure, aurait été d'au moins 13–13.5 kbar pour une température entre 550 et 600°C, selon le géobaromètre fondé sur la phengite. Pour l'unité supérieure, la pression maximale ne peut être précisée. Les relations texturales et les données sur la composition des minéraux nous informent à propos des conditions à divers stades de décompression des deux unités. Le tracé de l'exhumation de l'unité inférieure a été presque isothermique jusqu'à une profondeur d'environ 12 km de la surface. Dans le cas de l'unité supérieure, l'exhumation a procédé le long d'un tracé P–T indicatif de refroidissement. Ces différences seraient attribuables à un chevauchement de l'unité supérieure, d'une origine plus profonde, sur l'unité inférieure à profondeur, au cours de l'exhumation. Dans ce cas, l'unité supérieure a agi comme isolant déjà chaud, et a ainsi permis à l'unité inférieure de conserver la chaleur. Le tracé P–T de la zone de Rhodope montre des ressemblances importantes dans la forme avec celui d'autres zones à haute pression (les Alpes occidentales, la péninsule de Seward en Alaska, les Cyclades de la mer Égée, par exemple); c'est donc dire que des contraintes analogues, impliquant une exhumation tectonique rapide ou un chevauchement continu de matériaux froids, pourraient expliquer le refroidissement qui a accompagné l'exhumation.

(Traduit par la Rédaction)

Mots-clés: métapélites, métamorphisme à haute pression, faciès éclogite, zone de Rhodope, Grèce.

INTRODUCTION

Pelitic rocks develop a wide range of distinctive minerals that are valuable indicators of metamorphic conditions because of their sensitivity to changes in pressure and temperature. However, high-P metamorphic assemblages in metapelites associated with eclogites commonly are obliterated by later metamorphic events. Regional manifestations of eclogite P–T conditions in some pelitic metamorphic terranes are lacking, and evidence for high-P metamorphism must be gleaned from relict assemblages in metabasites. This differential overprinting, attributed to contrasting behavior of pelites and metabasites upon decompression, can result in a misinterpretation of the P–T evolution of pelitic rocks associated with eclogites. Recently, however, high-pressure metamorphism has been documented in pelitic rocks from several more or less extensively overprinted, polymetamorphic terranes around the world to reveal a common history with associated retrograded eclogites (*e.g.*, Heinrich 1982, Franz *et al.* 1986, Vuichard & Ballèvre 1988, Chopin *et al.* 1991).

The recent discovery of eclogite relics in the Rhodope zone (Liati 1986, Kolceva *et al.* 1986, Mposkos & Perdikatsis 1987, Liati & Mposkos 1990) prompted a re-investigation of metamorphism in the associated metapelites. The latter rocks also record high-pressure relics (Mposkos 1989a). The purpose of the present study is to construct a P–T path for the Rhodope polymetamorphic terrane, based on the sequences of mineral assemblages in metapelitic rocks, and the chemistry of these minerals. The arising metamorphic history is connected with that of the amphibolitized eclogites, which are concordantly interlayered with the metapelites studied.

The mineral abbreviations used in the present study are from Kretz (1983). In addition, the abbreviation "Phen" holds for phengite.

GEOLOGICAL SETTING

The Rhodope zone is a crystalline complex of uncertain age that lies between the Balkanides to the north and the Dinarides–Hellenides to the west-south-west. In Greece, the Rhodope zone occupies most of eastern Macedonia and Thrace (Fig. 1A). It is bounded against the Serbomacedonian Massif to the west by the Strimon line, a west-dipping thrust fault of Tertiary age (Kockel & Walther 1965, Burchfiel 1980), and by Mesozoic low-grade metamorphosed rocks of the Circum-Rhodope Belt on the east. The age of sedimentation is unknown; no fossils have been found in these metamorphic rocks.

The Rhodope zone is primarily composed of metamorphic rocks including quartzofeldspathic gneisses, migmatites, pelitic rocks, amphibolitized eclogites, marbles, calc-silicates and ultramafic rocks. Postmetamorphic Oligocene intrusive and extrusive rocks are abundant. Petrological studies (Liati 1986, Mposkos & Perdikatsis 1987, Mposkos 1989a, Liati & Mposkos 1990), combined with geochronology (K–Ar on metamorphic minerals: Liati 1986, Liati & Kreuzer 1990; lead isotope data from migmatites of the Bulgarian part: Arnaudov *et al.* 1990) revealed that the Rhodope was involved in an Alpine metamorphic cycle of high-pressure (eclogite-facies) metamorphism extensively overprinted under medium-pressure conditions in Eocene time. A low-pressure, greenschist-facies retrograde overprint marks the end of Alpine metamorphism.

Significant differences in metamorphic grade (on the order of 100°–150°C), for the medium-pressure overprinting event, identified in closely lying rocks (separated by a distance of less than 200 m) led to the delineation of an intervening discontinuity that subdivides the Rhodope zone into two major tectonic units (Fig. 1A): 1) the lower tectonic unit (hereafter called LTU), characterized by metamorphism at conditions of the upper greenschist to lower amphibolite facies, and 2) the upper tectonic unit (hereafter called UTU), characterized by medium to upper amphibolite-facies conditions.

Differences in lithology throughout the Rhodope zone are grossly marked by the abundance of thick units of marble (the so-called "Falakron marble") in the western part and the predominance of mafic and ultramafic rocks in the eastern parts of the zone. The LTU consists of augen gneisses (orthogneisses) as the lowermost lithologic formation, overlain by a series of alternating pelitic rocks and amphibolitized eclogites. Metadiabasic, metagabbroic and meta-aplitic dykes cross-cut the augen gneisses in eastern Rhodope. There, large ultramafic bodies are incorporated in the LTU. In western Rhodope, metadiabasic and ultramafic rocks are rare; large volumes of massive marble, banded toward the lower parts, constitute the uppermost lithologic formation. The UTU consists of migmatized augen gneiss at the base, overlain by alternations of pelitic rocks that contain amphibolitized eclogite and moderately thick units of marble. A dismembered ophiolite sequence including ultramafic, layered metagabbroic rocks and metadiorites is best developed in eastern Rhodope. Abundant granitic pegmatites cross-cut most rock types of the UTU, mainly in eastern and central Rhodope; pegmatites are absent from the LTU.

P–T conditions of high-pressure metamorphism in the LTU, as estimated in metabasic rocks and orthogneiss, are 550°–600°C and 14–15 kbar (Mposkos 1989a, b, Liati & Mposkos 1990). In the UTU, peak metamorphic conditions are uncertain because of the extended, high-grade metamorphic overprint. However, the presence of kyanite eclogites in central Rhodope near the Greek–Bulgarian border (Ardino area) suggests that pressures in the UTU possibly reached 18 kbar (Liati & Mposkos 1990).

The metapelites studied are intercalated within quartzofeldspathic rocks that ˙alternate concordantly
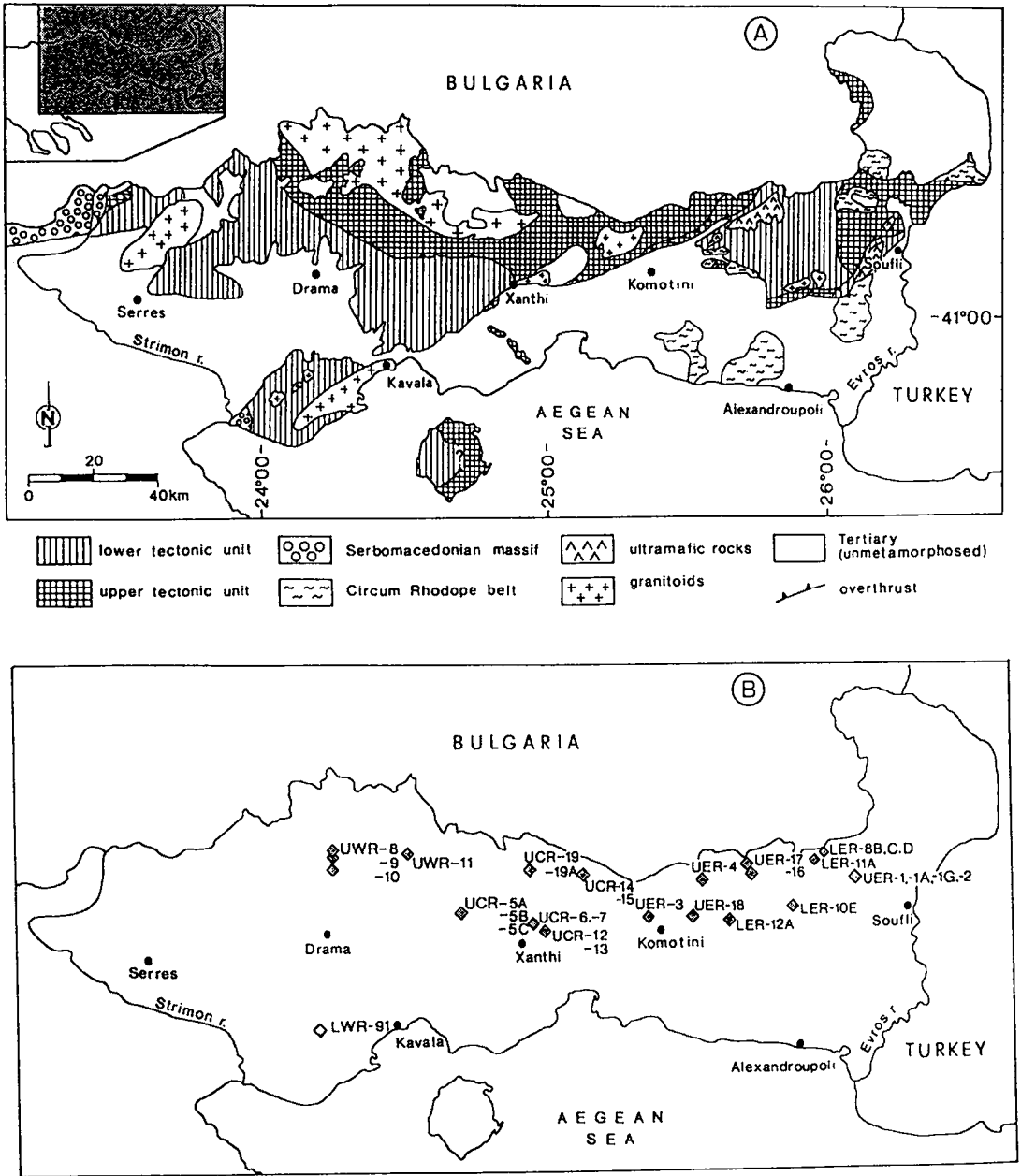
FIG. 1. (A) Simplified geological map of the Greek Rhodope; the two tectonic units are shown. (B) Location of sampled metapelites. Samples starting with "L" and "U" are from the lower tectonic unit and upper tectonic unit, respectively.

with amphibolitized eclogite and marble. The mineral assemblages developed and the mineral chemistry of the pelitic rocks differ in the two tectonic units; therefore, these themes are examined separately in each tectonic unit.

METAPELITES OF THE LOWER TECTONIC UNIT

Petrography

The metapelitic rocks of the LTU consist of garnet –

TABLE 1. REPRESENTATIVE SAMPLES SHOWING THE SEQUENCES OF MINERAL ASSEMBLAGES IN THE METAPELITES OF THE LOWER TECTONIC UNIT, WHICH CHARACTERIZE THE DIFFERENT STAGES OF THE METAMORPHIC EVOLUTION

| | Prograde path and peak metam.cond. | | | | | | | | Exhumation path | | | | | | | |
| | stage 1 | | | | | | | | stage 2 and 3 | | | | | stage 4 | | |
Sample Nr.	Qtz	Cld	Grt	Chl$_1$	Phen	Pg	Ky	Rt	Ms	Chl$_2$	Ilm	St	Bt	And	Chl$_3$	Ms$_3$
LER–10E	+	+	+	+	+	+		+	+						+	
LWR–90	+	+	+	+	+			+	+		+					
LER–11A	+	+	+	+	+	+		+	+	+		+	+			
LER–8B	+	+	+	+	+	+	+	+	+	+	+	+	+	+	+	
LER–12A	+	(i)	+		+			+	+	+		+				+
LER–13	+		+	+				+	+			+	+		+	+
LWR–91	+		+	+	+			+	+		+	+	+			

Samples LER–10E, LWR–90, LER–11A, LER–8B and LER–12A represent metapelites of "Type 1", whereas LER–13 and LWR–91 represent metapelites of "Type 2". (i): inclusion in garnet.

chloritoid ± staurolite mica schist. Based on their characteristic mineral assemblages, these rocks can be distinguished into the following two types (summarized also in Table 1).

(1) *Metapelites of "type 1"*: They are represented by the mineral assemblages (a) garnet – chloritoid – chlorite – white K-mica ± paragonite – quartz – rutile ± ilmenite, which is common in the southern part of eastern Rhodope and occurs rarely in western Rhodope (*i.e.*, samples LER–10E, LWR–90; Fig. 1B), and (b) garnet – chloritoid – staurolite – chlorite – white K-mica ± paragonite ± biotite ± kyanite – quartz – rutile ± ilmenite, which is common in the northwestern part of eastern Rhodope (*i.e.*, samples LER–11A, LER–8B, LER–8C, LER–8D, LER–12A; Fig. 1B).

In these rocks, garnet occurs commonly as porphyroblasts with inclusions of quartz, rutile and chloritoid. Two generations of chlorite are recognized in the metapelites characterized by mineral assemblage (a): primary chlorite (chlorite$_1$), which coexists with garnet + chloritoid + high-Si phengite, and a late-stage retrograde chlorite (chlorite$_3$), which replaces garnet or chloritoid. As shown below, the two types of chlorite differ also in their chemical composition; chlorite$_1$ is richer in Mg than chlorite$_3$. In the metapelites with mineral assemblage (b), staurolite appears as a new mineral; it grows at the expense of chloritoid (Figs. 2A, C). Three generations of chlorite are recognized in these rocks: primary chlorite (chlorite$_1$) which, like in the metapelites of mineral assemblage (a), coexists with garnet + chloritoid + high-Si phengite, an intermediate generation (chlorite$_2$) not identified in the pelitic rocks with mineral assemblage (a), which together with staurolite grows at the expense of chloritoid, and the late-stage retrograde chlorite$_3$, which replaces garnet or chloritoid. In a few samples, kyanite is associated with chloritoid and chlorite$_1$ and replaced by staurolite. Biotite forms with staurolite at the expense of chloritoid (Fig. 2B). In the kyanite-bearing metapelites, andalusite + chlorite$_3$ replace chloritoid (Fig. 2C).

(2) *Metapelites of "type 2"*: They are represented by the mineral assemblage garnet – staurolite – chlorite – white K-mica – biotite – albite – quartz – rutile ± ilmenite, which is common in the western and northwestern part of eastern Rhodope (*i.e.*, sample LER–13) and rarely observed in western Rhodope (Pangaeon Mountain) (*i.e.*, sample LWR–91) (Fig. 1B). Chloritoid is absent in this type of pelite. Staurolite appears together with biotite and chlorite, commonly around resorbed porphyroblasts of garnet.

MINERAL CHEMISTRY

Garnet

Garnet shows growth zoning, with an increase in Fe and Mg and a decrease in Mn and Ca from core to rim (Table 2, Fig. 3). This pattern of zoning is typical for garnet found in all types of pelite in the LTU.

Chloritoid

Chloritoid is generally zoned; a slight increase in Mg and decrease in Mn from core to rim is noted (Table 2). Differences in chemical composition are observed also between chloritoid inclusions in garnet and matrix chloritoid, the latter being richer in Mg and poorer in Mn than the former (compare compositions for sample LER–8B, Table 2). Systematic changes in the Mg/Fe ratio of neighboring points of chloritoid inclusions and host garnet indicate chemical equilibrium between the two minerals (see Mposkos 1989a, for details).

White micas

Potassic white micas vary in composition from high-Si phengite (Si up to 6.87 atoms p.f.u.) to pure muscovite (Table 3). The Si content of the white K-mica decreases with increasing intensity of overprint. An excess Mg + Fe$_{tot}$ beyond the requirement of the phengite
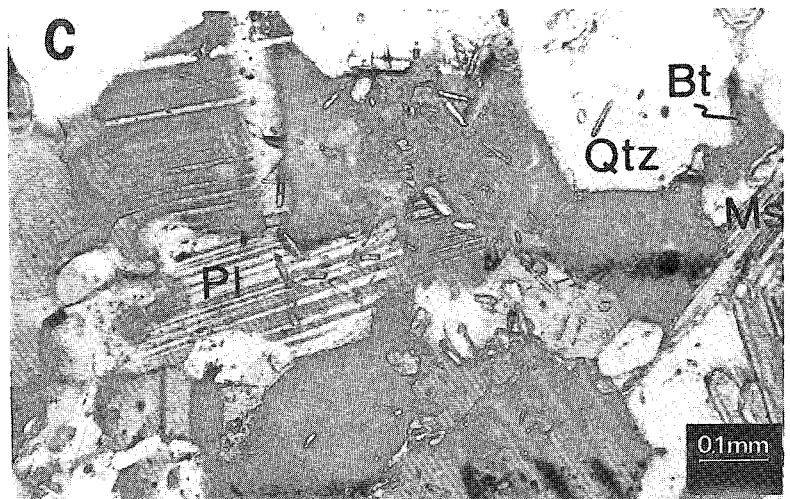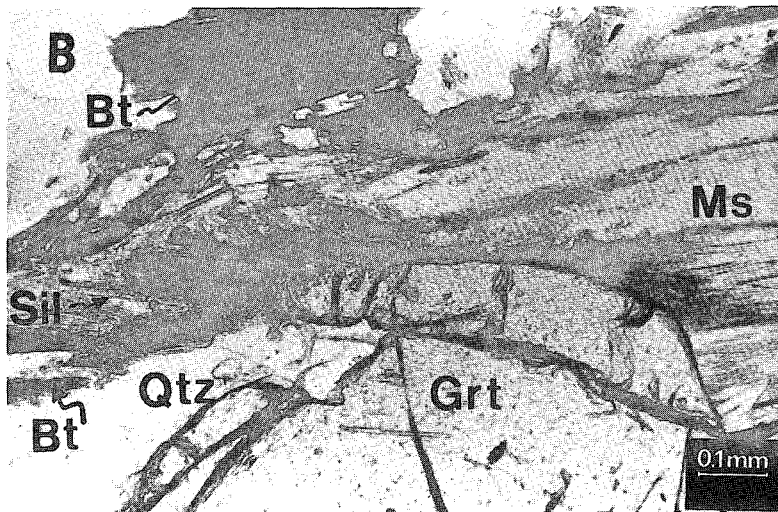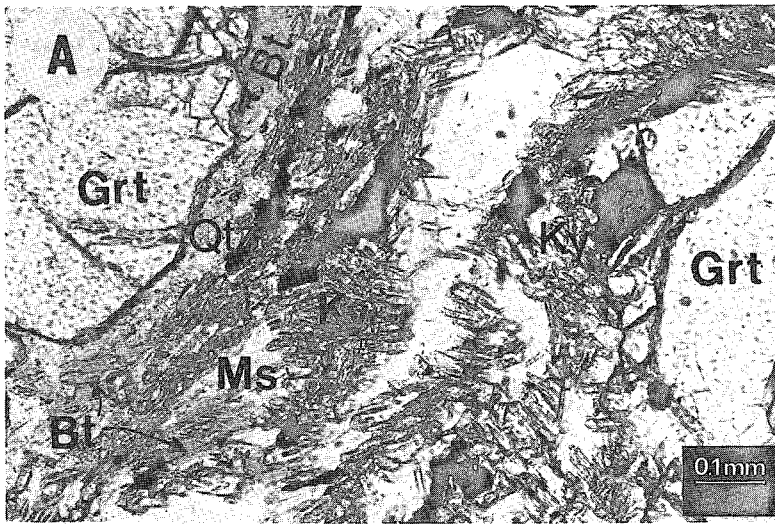
FIG. 2. Photomicrographs of pelitic rocks of the LTU. (A) Newly formed staurolite which, together with chlorite$_2$, muscovite and quartz, grew at the expense of chloritoid (reaction 1), (B) chloritoid replaced by staurolite + biotite (reaction 2), (C) chloritoid replaced by staurolite + chlorite$_2$ + muscovite (reaction 1) and in a later stage by andalusite + chlorite$_3$ (reaction 3).

TABLE 2. REPRESENTATIVE ELECTRON-MICROPROBE DATA ON GARNET AND CHLORITOID FROM THE LOWER TECTONIC UNIT

	LER-10E		LER-8B		LER-12	LER-8B		
	1(c)	2(r)	3(c)	4(r)	5	6(c)	7(r)	8(i)
SiO$_2$	37.04	37.10	37.46	37.09	37.05	24.77	25.18	24.76
TiO$_2$	0.13	-	-	-	0.05	-	-	-
Al$_2$O$_3$	21.22	21.14	21.13	21.38	20.98	41.66	41.22	39.63
Fe$_2$O$_3$	-	-	-	-	-	-	-	-
FeO	25.94	33.80	23.80	30.52	36.34	22.93	22.55	25.46
MnO	8.35	2.25	7.27	4.26	2.12	0.39	0.36	0.96
MgO	1.09	2.47	1.49	2.67	2.64	4.13	4.70	2.71
CaO	6.38	3.23	8.59	4.00	0.89	-	-	-
Total	99.70	99.99	99.92	99.92	100.07	93.88	94.01	93.58

Cations on the basis of 24 oxygen atoms

Si	5.968	5.978	5.994	5.959	5.994	4.000	4.005	4.076
^{IV}Al	0.032	0.022	0.006	0.041	0.006	-	-	-
^{VI}Al	3.997	3.992	3.980	4.007	3.995	7.917	7.805	7.688
Ti	0.016	-	0.022	-	0.006	-	-	-
Fe^{3+}	-	-	-	-	-	-	-	-
Fe^{2+}	3.495	4.561	3.185	4.100	4.918	3.092	3.029	3.504
Mn	1.142	0.308	0.986	0.580	0.290	0.053	0.049	0.135
Mg	0.261	0.593	0.356	0.639	0.637	0.993	1.125	0.677
Ca	1.101	0.557	1.473	0.689	0.154	-	-	-
X_{Mg}	0.07	0.12	0.10	0.13	0.11	0.24	0.27	0.16

Analyses 1–5: garnet, 6–8: chloritoid; (c) core, (r) rim; number 8: inclusion of chloritoid in garnet. Compositions of garnet were recalculated for Fe^{3+}. Compositions expressed as wt% oxides.

TABLE 3. REPRESENTATIVE ELECTRON-MICROPROBE DATA ON WHITE MICAS FROM THE LOWER TECTONIC UNIT

	LER-10E		LER-11A				LER-8B	
	1(c)	2(r)	3(c)	4(c-r)	5(r)	6	7(c)	8(r)
SiO$_2$	51.80	49.07	51.89	48.38	47.15	48.64	52.33	47.91
TiO$_2$	0.38	0.37	0.24	0.35	0.36	0.03	0.25	0.34
Al$_2$O$_3$	27.77	34.16	27.35	33.24	37.95	39.53	26.98	35.32
FeO*	2.22	0.94	2.52	2.37	0.89	0.38	3.01	1.36
MnO	0.08	0.05	-	0.04	-	-	-	-
MgO	3.42	1.52	3.63	1.71	0.36	0.12	3.30	1.08
Na$_2$O	0.60	1.31	0.36	1.01	2.26	7.48	0.48	1.61
K$_2$O	10.62	9.58	10.87	9.92	8.03	0.70	10.76	9.44
Total	96.89	97.02	96.86	97.02	97.00	96.88	97.11	97.06

Cations on the basis of 22 oxygen atoms

Si	6.818	6.379	6.823	6.339	6.092	6.097	6.872	6.232
^{IV}Al	1.182	1.621	1.177	1.661	1.908	1.909	1.128	1.767
^{VI}Al	3.127	3.613	3.061	3.470	3.871	3.937	3.046	3.647
Ti	0.038	0.036	0.024	0.034	0.035	0.002	0.025	0.033
Fe	0.244	0.102	0.277	0.259	0.097	0.040	0.330	0.148
Mn	0.009	0.006	-	0.004	-	-	-	-
Mg	0.671	0.295	0.711	0.333	0.070	0.022	0.646	0.209
Na	0.152	0.331	0.091	0.256	0.570	1.817	0.123	0.407
K	1.784	1.589	1.826	1.659	1.328	0.111	1.802	1.567

Analysis number 6: paragonite. (c) core, (r) rim, (c-r) between core and rim; FeO*: total iron as FeO. Compositions expressed as wt% oxides.
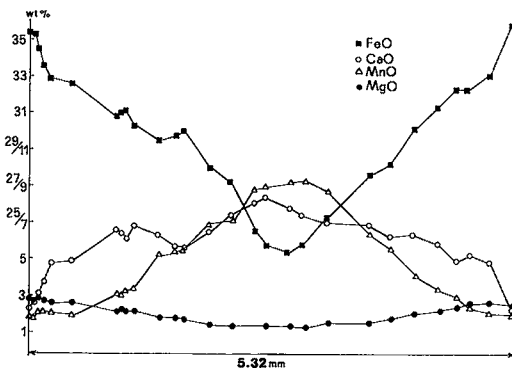

FIG. 3. Representative zoning profile of garnet from the pelitic rocks of the LTU showing a typical "growth zoning" pattern of a garnet porphyroblast (sample LER–11A).

substitution is observed in some crystals, which indicates that part of the iron may be trivalent, substituting for Al. Zoning is characterized by a continuous decrease in Si toward the rim, from 6.82 to 6.09 (i.e., sample LER–11A, analyses 4, 5 and 6 of Table 3). A record of the high-pressure and decompression conditions of metamorphism can therefore be preserved in a single

crystal of potassic white mica. Figure 4 illustrates a comparative plot of the phengite and muscovite compositions from one pelitic rock from the LTU, in terms of Al$_{tot}$ versus Si (A) and Al$_{tot}$ versus Na/(Na + K) (B). As is shown in Figure 4B, the paragonite component of the white K-mica is low in Si-rich phengite and higher in muscovite. This inverse correlation of Na with the celadonite component of potassic white mica has already been widely observed (e.g., Cimmino & Messiga 1979, Chopin & Maluski 1980, Heinrich 1982, Guidotti 1984, Evans & Patrick 1987, Mposkos 1989a) and is consistent with the reluctance of natural paragonite to accommodate more Si than the ideal 6 atoms per formula unit. The increase in paragonite content accompanying the change from phengite to muscovite during decompression of the LTU is therefore a crystal-chemical effect (see Guidotti 1984, p. 382).

Paragonite contains 4 to 12 mol% of the muscovite component. Paragonite poor in the muscovite end-member (Table 3, analysis 6) coexists with high-Si phengite, whereas that richer in muscovite (9–12 mol%) coexists with less phengitic white K-mica. This indicates that paragonite, like potassic white mica, re-equilibrates during unloading.

Staurolite

Staurolite is characterized by X_{Mg} values between 0.10 and 0.18 (Table 4). The compositions of staurolite (and chlorite) richer in Fe in sample LER–12A, which
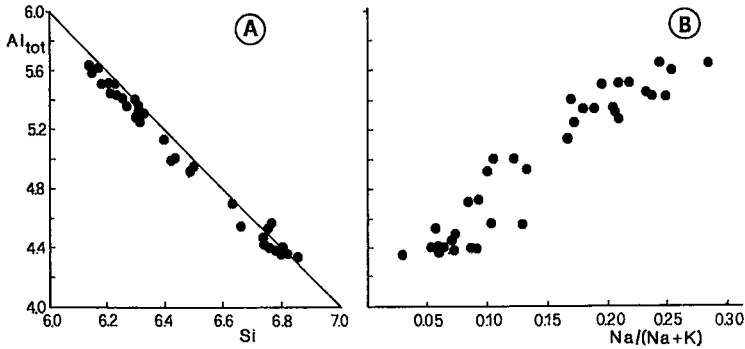
FIG. 4. Compositional variation in potassic white mica from a representative sample (LER–11A) of the pelitic rocks of the LTU. A. Al_{tot} *versus* Si; B. Al_{tot} *versus* Na/(Na + K). High-Si phengite is characterized by a low Na/(Na + K) ratio (compare A and B). See text for details.

contains only a few relics of chloritoid, are attributed to progress of the reaction Cld + Phen = St + Chl + Ms + Qtz + H_2O, which is responsible for the formation of staurolite (see below). A slight increase in Fe from core to rim is observed in some zoned grains of staurolite.

TABLE 4. REPRESENTATIVE ELECTRON-MICROPROBE DATA ON STAUROLITE AND BIOTITE FROM THE LOWER TECTONIC UNIT

	LER-8B		LER-12A		LER-8B	
	1	2	3	4	5	6
SiO_2	28.14	28.41	27.98	28.11	35.26	38.35
TiO_2	0.41	0.41	0.52	0.41	1.37	1.41
Al_2O_3	53.60	54.00	54.54	53.85	19.80	20.30
FeO^*	13.43	12.75	13.38	12.59	19.56	16.86
MnO	0.24	0.25	0.39	0.22	0.03	0.06
MgO	1.73	1.05	0.80	1.02	9.94	9.12
Na_2O	-	-	-	-	0.22	0.13
K_2O	-	-	-	-	9.84	10.06
ZnO	0.37	1.15	0.25	0.45	-	-
Total	97.92	98.02	97.86	96.65	95.99	96.95

Cations on the basis of

	47(O)				22(O)	
Si	7.968	8.030	7.886	8.026	5.352	5.630
Al	17.890	17.993	18.118	18.119	3.543	3.519
Ti	0.087	0.088	0.110	0.088	0.156	0.156
Fe	3.181	3.014	3.153	3.006	2.483	2.079
Mn	0.058	0.060	0.094	0.053	0.004	0.074
Mg	0.730	0.444	0.336	0.434	2.249	1.999
Na	-	-	-	-	0.064	0.037
K	-	-	-	-	1.906	1.891
Zn	0.078	0.239	0.052	0.095	-	-
X_{Mg}	0.18	0.13	0.10	0.13	0.48	0.49

Analyses 1–4: staurolite, 5, 6: biotite. Analyses 1, 2: in contact with chloritoid and chlorite$_2$; 3: staurolite rim against chlorite$_2$. FeO^*: total iron as FeO. Compositions expressed in wt% oxides.

Biotite

Biotite, which appears in the metapelites of "Type 1" with mineral assemblage (b), is characterized by X_{Mg} values of about 0.48 (Table 4). It is formed, together with staurolite, at the expense of chloritoid during the stage of exhumation (see below, reaction 2).

Chlorite

The types of chlorite distinguished on textural grounds differ in their chemical composition (Table 5). In the first type of metapelites, primary chlorite (chlorite$_1$), which belongs to the paragenesis Grt + Cld + Chl + Phen, displays higher X_{Mg} values than chlorite$_2$ which, together with staurolite, forms at the expense of chloritoid. Chlorite$_2$ is characterized in turn by higher X_{Mg} values than the late-stage retrograde chlorite$_3$, which replaces garnet or chloritoid (compare chlorite compositions of sample LER–8B, Table 5). The highest X_{Mg} values were obtained for chlorite coexisting with the highest-Si phengite.

Petrological interpretation of the textural and mineral chemical data

(1) Metapelites of "Type 1": The stable and systematic coexistence of high-Si phengite with Grt + Cld + Chl$_1$ indicates that the assemblage Grt + Cld + Chl$_1$ + Phen + Pg + Rt + Qtz, which is common in this type of metapelite, is related to the high-pressure event. In the metapelites exhibiting mineral assemblage (b), the white K-mica that is in direct contact with Grt + Cld + Chl$_1$ is a high-Si phengite, whereas that in textural equilibrium with staurolite is significantly poorer in the celadonite component. The mineral association Grt + Cld + Chl, common in medium-pressure metapelites from other

TABLE 5. REPRESENTATIVE ELECTRON-MICROPROBE DATA ON CHLORITE FROM THE LOWER TECTONIC UNIT

	LER-10E		LER-12A	LER-8B		
	1	2	3	4	5	6
SiO_2	24.29	22.60	23.78	27.85	24.90	23.05
TiO_2	0.10	0.20	0.08	0.04	0.06	0.05
Al_2O_3	20.82	18.09	22.26	19.67	23.07	20.47
FeO^*	27.81	37.25	29.74	22.20	25.80	37.32
MnO	0.09	1.06	0.19	0.16	0.17	1.31
MgO	14.02	3.69	10.82	17.00	13.31	4.94
Na_2O	-	0.16	-	-	-	-
Total	87.13	86.89	86.87	87.52	87.11	87.21

Cations on the basis of 28 oxygen atoms

Si	5.242	5.488	5.194	5.794	5.279	5.287
^{IV}Al	2.758	2.512	2.806	2.206	2.721	2.713
^{VI}Al	2.537	2.665	2.922	2.618	3.044	2.818
Ti	0.015	0.037	0.126	0.007	0.010	0.009
Fe	5.019	7.565	5.422	3.863	4.538	7.157
Mn	0.015	0.218	0.035	0.028	0.030	0.266
Mg	4.508	1.334	3.521	5.272	4.206	1.690
Na	-	0.075	-	-	-	-
X_{Mg}	0.47	0.15	0.39	0.58	0.48	0.19

Analyses 1 and 4: chlorite$_1$, 3 and 5: chlorite$_2$, 2 and 6: chlorite$_3$. FeO^*: total iron as FeO. Compositions expressed as wt% oxides.

areas, has also been reported in eclogitic metapelites of several polymetamorphic terranes, *e.g.*, New Caledonia (Ghent *et al.* 1987), the Hohe Tauern Window (Miller 1977, Spear & Franz 1986), the Massif Central (Délor *et al.* 1987), and the Sesia zone (Vuichard & Ballèvre 1988). The coexistence of staurolite with white K-mica poor in celadonite component in these metapelites implies that formation of staurolite is related to the medium-pressure overprint. According to the textural observations described previously, staurolite grows at the expense of chloritoid, possibly according to the reaction:

$$Cld + Phen = St + Chl + Ms + Qtz + H_2O \qquad (1)$$

Where staurolite grows together with biotite at the expense of chloritoid, the reaction:

$$Cld + Ms + Qtz = St + Bt + H_2O \qquad (2)$$
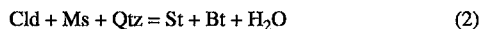
may have taken place. Staurolite associated with chloritoid occurs in metapelites of the LTU located only in the northwestern part of eastern Rhodope. In chloritoid-bearing metapelites of the southeastern part of eastern Rhodope and of western Rhodope, staurolite is absent. This finding indicates that in the areas where chloritoid-bearing metapelites lack staurolite, metamorphic conditions were of lower grade.

Chloritization of biotite and sericitization of staurolite

are apparently related to late-stage retrograde processes. In the kyanite-bearing metapelites (sample LER–8B; Table 1), the replacement of chloritoid by andalusite + chlorite$_3$ takes place during the same retrograde stage of metamorphism, according to the reaction:

$$Cld + Qtz = And + Chl + H_2O \qquad (3)$$
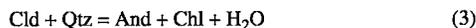
(2) Metapelites of "Type 2": In this type of metapelite, the formation of staurolite is possibly related to the reaction:

$$Grt + Chl + Ms = St + Bt + H_2O \qquad (4)$$
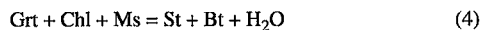
as is suggested by the textural relations of the minerals involved.

PHASE RELATIONS

The metapelite assemblages can be described by the system K_2O–FeO–MgO–Al_2O_3–SiO_2–H_2O (KFMASH). AFM topologies for the metapelites were projected according to Thompson (1957), taking into account the presence of quartz, white K-mica, paragonite, rutile, ilmenite, and H_2O (Fig. 5). The three-phase assemblage Grt – Cld – Chl predominates in pelitic rocks. Projected phase relations for the high-pressure stage are shown in Figure 5A for two samples (LER–10E, circles, and LER–8B, triangles). The two-phase assemblage Cld–Grt corresponds to chloritoid inclusions in a garnet core (line 1) and a garnet rim (line 2). The shifting of line (2) toward more magnesian compositions between samples LER–10E and LER–8B indicates garnet growth at the expense of chloritoid (+ chlorite) during prograde metamorphism. The minerals constituting the three-phase high-pressure assemblage Grt – Cld – Chl in the matrix of sample LER–10E show still higher X_{Mg}. Garnet, chloritoid, and chlorite are more magnesian in sample LER–8B than in LER–10E. In sample LER–8B, the coexisting high-Si phengite is the richest in celadonite component of the samples studied. Sample LER–8B also contains the high-pressure paragenesis Ky – Cld – Chl. Given the relative position of the representative samples LER–8B and LER–10E in the field (Fig. 1B), and taking into account the AFM diagram of Figure 5A and the Si-rich composition of the phengite in LER–8B, an increase in both temperature and pressure can be inferred from south to north, in eastern Rhodope. The lack of critical high-pressure talc-bearing paragenesis (such as those reported for other areas, *i.e.*, Chopin & Schreyer 1983, Goffé & Chopin 1986) in the Rhodope metapelites is apparently a consequence of their "normal", more Fe-rich composition than the one required for the formation of this mineral.

Figures 5B and 5C illustrate the three-phase AFM parageneses related to the medium-pressure overprint. In these rocks, staurolite formed at the expense of chloritoid (reaction 1) and kyanite. The chlorite in Figure
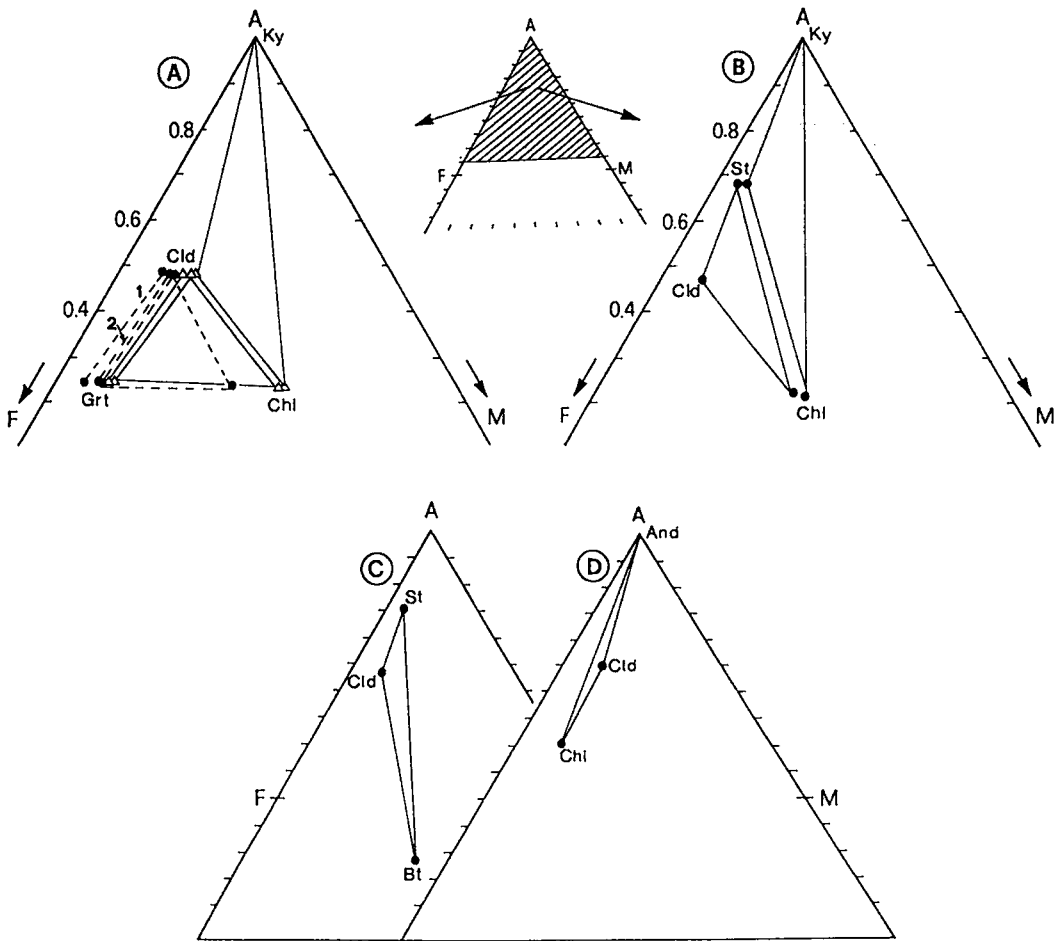
FIG. 5. AFM projections of assemblages that coexist with potassic white mica – quartz – paragonite – rutile ± ilmenite – H$_2$O in the pelitic rocks of the LTU. In (A), dashed lines (1) and (2) are from chloritoid inclusions in garnet core and rim, respectively. In the same diagram, circles correspond to sample LER–10E, and triangles to LER–8B. Diagram (A) corresponds to the high-pressure stage, (B) and (C) to the medium-pressure overprint, and (D) to the latest retrograde steps of the greenschist facies. See text for details.

5B is chlorite$_2$ (see "Petrography"), which is poorer in Mg than chlorite$_1$ in Figure 5A. The three-phase AFM paragenesis Cld – St – Bt illustrated in Figure 5C corresponds to a more advanced stage of the exhumation. Finally, Figure 5D shows the latest retrograde steps of the exhumation, with the three-phase paragenesis Cld – And – Chl.

METAPELITES OF THE UPPER TECTONIC UNIT

Petrography

The metapelites of the UTU generally consist of garnet – kyanite ± staurolite gneiss and schist. Based on their characteristic mineral assemblages, these rocks can be distinguished into two types (summarized also in Table 6).

(1) Metapelites of "Type 1": They are represented by the mineral assemblages (a) garnet – kyanite – staurolite – chlorite – muscovite – quartz – rutile ± ilmenite, which is common in the easternmost part of Rhodope (*i.e.*, samples UER–1A, UER–1G, UER–2; Fig. 1B), and (b) garnet – kyanite – staurolite ± sillimanite – biotite – muscovite – quartz ± plagioclase – rutile ± ilmenite, which occurs in the areas northwest of Komotini, eastern Rhodope (*i.e.*, samples UER–3, UER–4), southwest of

TABLE 6. REPRESENTATIVE SAMPLES SHOWING THE SEQUENCES OF MINERAL ASSEMBLAGES IN THE METAPELITES OF THE UPPER TECTONIC UNIT, WHICH CHARACTERIZE THE DIFFERENT STAGES OF THE METAMORPHIC EVOLUTION

| Sample Nr. | Prograde path and peak metam. cond. | | | | | | | | | Exhumation path | | | | | | | | | | | | | |
| | stage 1 | | | | | | | | | stage 2, 2a and 3 | | | | | | | stage 4 | | | late retrograde stage | | | |
	Qtz	Grt	Ky1	St1	Bt1	Ms1	Chl1	Ilm1	Rt	Ky2	Bt2	Pl	St2	Ilm2	Chl2	Ms2	Bt2	Sil	Kfs	Bt3	Ms3	Chl3	And
UER-1A	+	+	+			+	(i)		+				+	+		+					+		
UER-1G	+	+	+		(i)	+	(i)		+				+	+	+	+					+		
UER-3	+	+				+			+		+	+	+	(i)		+					+	+	
UER-4	+	+	+		+	+			+		+	+				+					+		+
UCR-5A	+	+	+		(i)	+			+		+		+	(i)				+			+		
UCR-5C	+	+	+	(i)	(i)	+		(i)	+		+		+	+				+					
UCR-6	+	+	+		+	+			+		+	+	+			+	+	+		+		+	
UWR-8E	+	+	+		+	+			+	+	+	+								+		+	
UCR-12	+	+	+		+	+			+	+	+	+						+				+	
UCR-15	+	+	+		+	+			+	+	+	+						+					
UER-16	+	+	+		+	+			+	+	+	+				+				+			
UCR-19	+	+	+		+				+				+					+	+	+		+	

Samples UER-1A, UER-1G, UER-3, UER-4, UCR-5A, UCR-5C and UCR-6 represent metapelites of "Type 1", whereas UWR-8E, UCR-12, UCR-15, UER-16 and UCR-19 represent metapelites of "Type 2". (i): inclusion in garnet, kyanite, staurolite.

Paranesti and north of Xanthi, central Rhodope (*i.e.*, samples UCR-5A, UCR-5B, UCR-5C, UCR-6, UCR-7; Fig. 1B).

In metapelites of "Type 1" with mineral assemblage (a), garnet is typically medium grained and shows resorbed edges. In some cases, it appears as porphyroblasts containing inclusions of kyanite, chlorite, muscovite, quartz, and rutile (Fig. 6A). In one garnet porphyroblast of sample UER-1G, a kyanite inclusion in garnet itself contains inclusions of garnet + phlogopite (Fig. 6A). Kyanite appears as prismatic porphyroblasts and is commonly replaced by muscovite and staurolite. Staurolite either surrounds resorbed crystals of kyanite or grows epitactically on them. Relics of resorbed kyanite are commonly found within staurolite. Moreover, staurolite coexists with garnet and chlorite (Fig. 6B). Chlorite is observed both as an inclusion in garnet and in the matrix. Matrix chlorite is retrograde, having formed at the expense of garnet. Two generations of muscovite are distinguished: the first appears as large flakes oriented within the foliation; it is rich in Ti (see "Mineral chemistry"), and may contain numerous inclusions of sagenitic rutile (oriented, net-forming fine needles of rutile). The second generation of muscovite forms small flakes that are not oriented with respect to the foliation, and is significantly poorer in Ti than the coarse-grained muscovite; it is formed by replacement of kyanite and of staurolite.

In the same type of metapelite with mineral assemblage (b), especially in samples UCR-6 and UCR-7, garnet and kyanite are unusually coarse grained. The common size of kyanite is 2–3 cm; crystals up to 10 cm long were observed. The garnet crystals, with a diameter commonly reaching 5 cm, are intensely deformed, with resorbed edges, and contain abundant inclusions of kyanite, rutile, quartz, and muscovite. The garnet grains commonly have a lenticular shape, with the long axis parallel to the schistosity of the rock. In sample UCR-5, staurolite (locally with ilmenite inclusions), ilmenite, rutile, and quartz were found within a few porphyroblasts of garnet. Ilmenite and staurolite with ilmenite inclusions are observed only in the core of the garnet crystals; toward the outer part of the same garnet crystals, only rutile is found (Fig. 6C). Staurolite of sample UCR-5 occurs both as an inclusion in garnet (staurolite₁), as well as in the matrix (staurolite₂). The matrix staurolite of this sample, as well as that of samples UCR-5A, UCR-5B and UER-3, contains inclusions of garnet, quartz, rutile and rare ilmenite, biotite and muscovite (Fig. 6D). Some ilmenite inclusions contain relics of rutile. Such ilmenite is probably retrograde (ilmenite₂ of Table 6). Kyanite appears as porphyroblasts with inclusions of biotite, quartz, and muscovite and is commonly replaced by muscovite. It is usually deformed, showing signs of bending and undulose extinction. In samples UCR-6 and UCR-7, kyanite is replaced by staurolite (Fig. 6E). In these samples, staurolite is itself replaced by sillimanite + biotite (Fig. 6F). Finally, in sample UER-4, kyanite was found to be partly replaced by andalusite and fine-grained muscovite.

(2) Metapelites of "Type 2": They are represented by the mineral assemblages (a) garnet – kyanite – biotite – muscovite – plagioclase – quartz ± sillimanite – rutile, which is widespread throughout the Rhodope zone (*i.e.*, samples UWR-8E, UWR-9, UWR-10 and UWR-11 in
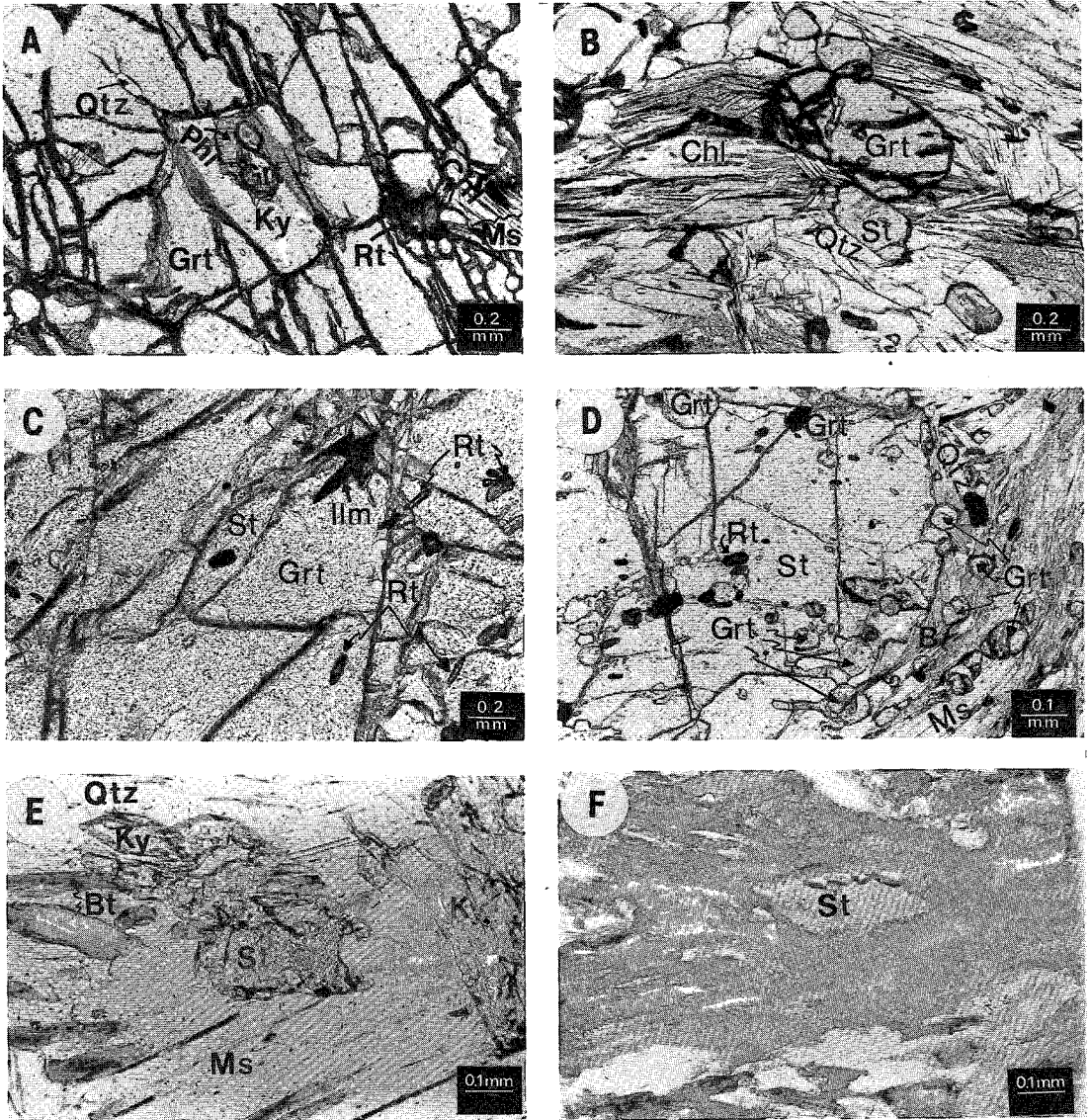
FIG. 6. Photomicrographs from the pelitic rocks of the UTU. (A) Garnet porphyroblast with inclusions of kyanite, chlorite, muscovite, quartz and rutile; a kyanite inclusion that itself encloses phlogopite + garnet; (B) staurolite + chlorite + quartz that grew at the expense of garnet (reaction 6); (C) staurolite inclusion in a garnet porphyroblast; ilmenite (dark mineral) appears as inclusion in staurolite and in the core of garnet, whereas rutile appears toward the outer part of the garnet crystal; (D) staurolite porphyroblast with garnet inclusions; garnet relics outside the staurolite crystal together with muscovite and biotite, replaced by staurolite + biotite (reaction 8); (E) kyanite replaced by staurolite (reaction 9); (F) staurolite replaced by sillimanite + biotite (dark minerals surrounding staurolite) (reaction 10).

the western part, UCR–12, UCR–13, UCR–14 and UCR–15 in the central part and UER–16, UER–17 and UER–18 in the eastern part of Rhodope; Fig. 1B), and (b) garnet – kyanite – sillimanite – biotite – plagioclase – K-feldspar – quartz – rutile, which occurs within the migmatite zone, in the area south of Thermes, central

Rhodope (i.e., samples UCR–19 and UCR–19A; Fig. 1B).

In this type of metapelite, two generations of kyanite were identified, on the basis of textural criteria. Kyanite$_1$ appears as deformed porphyroblasts with inclusions of garnet, biotite, rutile, and quartz. Kyanite$_2$ is present in
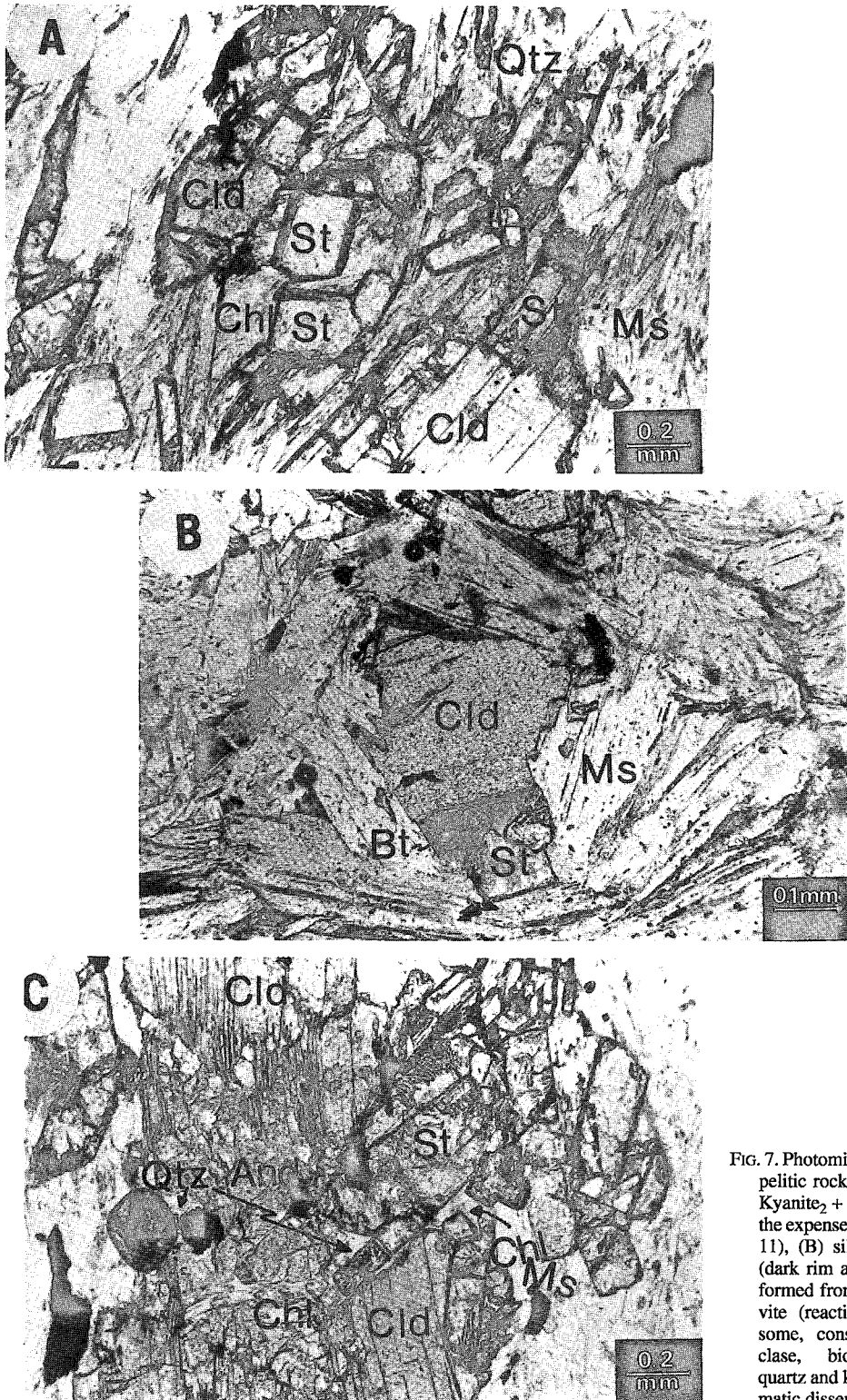
Fig. 7. Photomicrographs from the pelitic rocks of the UTU. (A) Kyanite$_2$ + biotite that grew at the expense of garnet (reaction 11), (B) sillimanite + biotite (dark rim around garnet) that formed from garnet + muscovite (reaction 14), (C) neosome, consisting of plagioclase, biotite, muscovite, quartz and kyanite (small prismatic disseminated crystals).

small crystals, typically in mutual contact with muscovite, biotite, and garnet (Fig. 7A). Garnet occurs as porphyroblasts with inclusions of biotite, kyanite$_1$, muscovite, plagioclase, rutile, and quartz, and rarely as inclusions in kyanite$_1$. It is noteworthy that plagioclase inclusions in garnet commonly contain inclusions of kyanite and quartz; kyanite and quartz seem to be resorbed by the plagioclase. These textural relationships suggest that plagioclase was possibly formed at the expense of garnet + kyanite + quartz + albite. Garnet shows resorbed edges and is commonly replaced by biotite and, in many cases, by biotite + kyanite$_2$ (Fig. 7A) or by biotite + plagioclase. Muscovite appears as large flakes that contain numerous inclusions of sagenitic rutile. Sillimanite, found both as "fibrolite" and as prismatic crystals, is abundant in samples UCR–14 and UCR–15. "Fibrolite" occurs commonly as felted masses, inside large flakes of muscovite, as well as around garnet crystals (Fig. 7B).

Signs of partial melting were identified in samples UER–16 and UER–17. In these samples, small pockets of neosome consist of aggregates of small unoriented grains of quartz, muscovite, biotite, equidimensional plagioclase and lenticular kyanite (Fig. 7C). Kyanite grains typically occur as inclusions in plagioclase and quartz. Granophyric intergrowths of plagioclase + quartz indicate contemporaneous crystallization of these minerals from the melt. Anatectic quartz and muscovite are easily distinguished from metamorphic counterparts on textural grounds: metamorphic quartz appears as large corroded grains and shows undulatory extinction; flakes of metamorphic muscovite also are corroded and oriented parallel to the foliation.

Green to pale brown biotite is found as a retrograde, greenschist-facies replacement of garnet + muscovite.

In metapelites of "Type 2" with mineral assemblage (b), kyanite occurs in large idiomorphic porphyroblasts that are replaced by symplectitic plagioclase at grain margins or, in some cases, are partially converted to sillimanite. Kyanite commonly contains inclusions of biotite, quartz, and rutile. Sillimanite appears as prismatic crystals associated with K-feldspar. Sericite (muscovite$_3$ of Table 6) and chlorite are formed as retrograde, greenschist-facies replacements of kyanite and biotite, respectively.

MINERAL CHEMISTRY

Garnet

In contrast to the grains of garnet of the LTU, which typically show growth zoning, those of the UTU are characterized by a variably developed retrograde zoning only toward the outermost rim (Table 7), depending on the mineral in contact with the rim. The rest of the crystal (core and inner rim) is generally homogeneous. According to Tracy (1982), homogenization of garnet is a result of volume diffusion due to high temperatures (>650°C).

TABLE 7. REPRESENTATIVE ELECTRON-MICROPROBE DATA ON GARNET FROM THE UPPER TECTONIC UNIT

	UER-16		UCR-5C		UCR-5A		UER-1G	
	1(c)	2(r)	3(c)	4(r)	5(c)	6(r)	7(c)	8(r)
SiO$_2$	38.27	37.60	36.54	37.41	36.48	36.51	37.91	37.70
TiO$_2$	0.04	-	-	-	0.20	0.25	-	-
Al$_2$O$_3$	21.69	21.30	21.21	21.46	21.40	21.07	21.60	21.32
FeO	28.48	31.97	34.80	33.42	34.65	34.79	31.02	33.65
Fe$_2$O$_3$	-	-	-	-	-	-	-	-
MnO	0.82	2.86	3.89	2.63	2.90	4.77	1.26	0.66
MgO	5.78	3.87	2.56	4.59	3.09	2.07	6.09	5.17
CaO	4.84	2.48	0.72	0.55	0.99	0.63	1.85	1.20
Total	99.92	100.08	99.72	100.06	99.71	100.09	99.73	99.70

Cations on the basis of 24 oxygen atoms

	1(c)	2(r)	3(c)	4(r)	5(c)	6(r)	7(c)	8(r)
Si	5.994	5.997	5.939	5.972	5.908	5.939	5.983	6.000
^{IV}Al	0.006	0.003	0.061	0.028	0.092	0.061	0.017	-
^{VI}Al	3.997	4.003	4.002	4.007	3.980	3.972	4.001	3.999
Ti	0.005	-	-	-	0.022	0.030	-	-
Fe^{3+}	-	-	-	-	-	-	-	-
Fe^{2+}	3.730	4.265	4.728	4.460	4.693	4.733	4.094	4.479
Mn	0.108	0.386	0.535	0.355	0.398	0.657	0.168	0.089
Mg	1.349	0.921	0.819	1.091	0.746	0.502	1.433	1.227
Ca	0.812	0.425	0.124	0.094	0.172	0.109	0.313	0.205
X$_{Mg}$	0.27	0.18	0.12	0.20	0.14	0.10	0.26	0.22

Analyses 5 and 6 pertain to inclusions in staurolite. (c) core, (r) rim; the garnet compositions were recalculated for Fe^{3+}. Compositions are expressed in wt% oxides.

The UTU was probably subjected to conditions of higher temperature during metamorphism than the LTU.

Figures 8A, B, C illustrate three representative compositional profiles of garnet from the metapelites of the UTU. These profiles are relatively flat except for the outer rim. The profile of Figure 8A corresponds to a garnet crystal in contact with biotite. The outermost rim of this garnet grain shows an abrupt decrease in Mg and increase in Fe, Ca and Mn. In Figure 8B, the profile illustrated pertains to an inclusion of garnet in staurolite. The decrease in Mg and increase in Fe, Mn observed in the outermost rim imply participation of garnet in the formation of staurolite (see below, reaction 8). Because X_{Mn}^{Gt} is greater than X_{Mn}^{St}, Mn enrichment in the outer rim of the garnet is attributed to diffusion of this element during consumption of the reacting garnet to form staurolite. Calcium, which is liberated from the garnet rim during reaction (8), diffuses into the remaining part of the crystal. Although no Ca increase is observed in the outermost rim, enrichment in this element is identified in an inner zone of the garnet crystal, possibly due to a higher rate of diffusion of Ca with respect to Mn. The profile of Figure 8C represents a garnet crystal with a homogeneous core. It shows a progressive, relatively smooth increase in Mg and Fe, and decrease in Ca toward the rim. This pattern reflects Ca diffusion as a result of the formation of plagioclase. The outermost rim of this grain shows an abrupt decrease in Mg, and
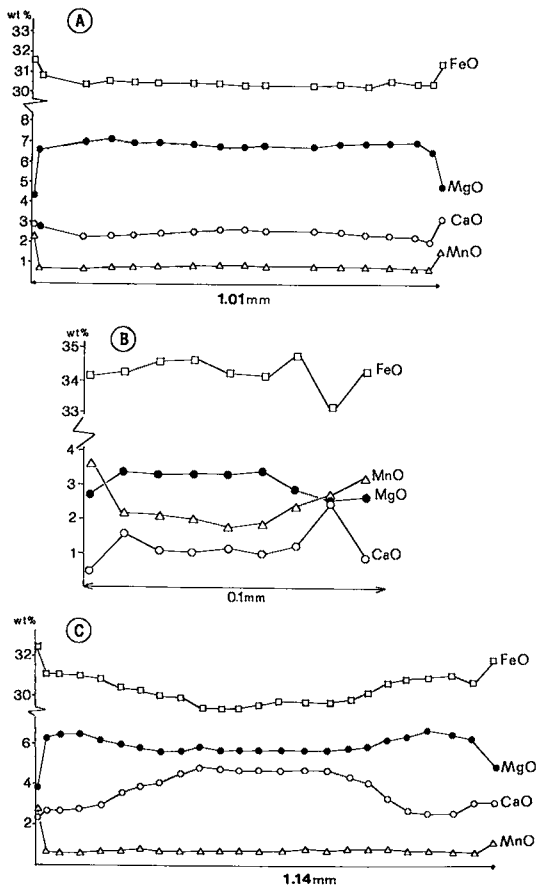
FIG. 8. Representative zoning profiles in garnet from the pelitic rocks of the UTU. (A) Flat pattern of a homogeneous garnet (sample UER–16) with reverse zoning only in the outermost rim, in contact with biotite + kyanite$_2$; (B) garnet inclusion in staurolite; the garnet is zoned only in the outer rim (sample UCR–5B); (C) relatively flat pattern in the core and regular increase of Mg, Fe and decrease in Ca toward the rim of a garnet porphyroblast (sample UER–16); the outermost rim shows the same pattern of zoning as (A). See text for details.

TABLE 8. REPRESENTATIVE ELECTRON-MICROPROBE DATA ON STAUROLITE FROM THE UPPER TECTONIC UNIT

	UCR-5A		UCR-5C			UER-1G		
	1(c)	2(r)	3	4	5(c)	6(r)	7(c)	8(r)
SiO$_2$	28.05	27.40	27.33	28.06	27.90	28.24	27.89	28.16
TiO$_2$	0.80	0.44	0.48	0.79	0.53	0.74	0.52	0.51
Al$_2$O$_3$	54.51	54.80	55.68	54.53	53.36	55.10	53.62	54.24
FeO*	12.12	12.11	12.42	12.13	11.55	11.36	10.32	10.60
MnO	-	0.22	0.32	-	-	-	0.18	-
MgO	2.24	1.50	1.25	2.24	2.86	2.64	2.49	1.57
ZnO	0.35	2.43	0.43	0.35	0.95	-	2.94	2.81
Total	98.07	98.90	97.91	98.10	97.15	98.08	97.96	97.89

Cations on the basis of 47 oxygen atoms

Si	7.875	7.733	7.708	7.875	7.941	7.880	7.920	7.913
Ti	0.168	0.093	0.102	0.168	0.113	0.155	0.111	0.108
Al	18.036	18.213	18.509	18.036	17.901	18.121	17.848	17.961
Fe	2.846	2.845	2.929	2.846	2.749	2.651	2.451	2.491
Mn	-	0.051	0.075	-	-	-	0.043	-
Mg	0.939	0.627	0.525	0.939	1.214	1.098	1.055	0.656
Zn	0.073	0.508	0.086	0.734	0.199	-	0.617	0.582
X_{Mg}	0.25	0.18	0.15	0.25	0.31	0.29	0.30	0.21

Analysis 3: inclusion in garnet core, 4: inclusion in garnet rim, 5, 6: replacing kyanite, 7, 8: in contact with garnet and chlorite. (c) core, (r) rim; FeO*: total iron as FeO. Compositions expressed as wt% oxides.

characterized by lower X_{Mg} values compared to those enclosed in the outer part of the same crystals (analysis 4). The staurolite inclusions probably grew in a prograde stage of metamorphic evolution. Staurolite in the matrix generally shows a decrease in X_{Mg} from core to rim. The rim composition is influenced by the mineral with which it is in contact. In metapelites of "Type 1" with mineral assemblage (a), higher X_{Mg} values are observed in the rim, where it is in contact with kyanite; the lowest X_{Mg} values in staurolite are found in the rim in contact with chlorite and garnet (compare analyses 6 and 8 of Table 8). In metapelites of "Type 1" with mineral assemblage (b) (samples UCR–5A, UCR–5B and UCR–5C), where staurolite is associated with garnet, biotite, and muscovite, the decrease in X_{Mg} value toward the rim of zoned crystals (Table 8, sample UCR–5A) suggests that staurolite formed at the expense of garnet + muscovite.

Muscovite

In the metapelites of the UTU, the potassic white mica is generally poor in celadonite component (Table 9). High-Si phengite was not preserved in the metapelites of the UTU, apparently because the temperature of the overprint exceeded the temperature of effective closure for celadonite exchange in white mica (see Dempster 1992). The common occurrence of small flakes of biotite surrounding large grains of muscovite or in parallel intergrowth with muscovite and quartz is consistent with the pre-existence of high-Si phengite. A characteristic of

increases in Fe and Mn. This profile is attributed to the participation of the garnet rim in the formation of biotite and kyanite (see below, reaction 11).

Staurolite

In the metapelites of the UTU, the composition of staurolite is controlled by the coexisting phases. Staurolite inclusions in cores of the garnet porphyroblasts of sample UCR–5C (see Table 8, analysis 3) are

TABLE 9. REPRESENTATIVE ELECTRON-MICROPROBE DATA ON MUSCOVITE FROM THE UPPER TECTONIC UNIT

	UER-1G					UWR-8E		UCR-7
	1	2(i)	3(i)	4	5	6	7	8
SiO$_2$	46.95	48.05	46.15	46.87	46.89	47.37	47.22	48.31
TiO$_2$	1.58	1.29	2.12	0.25	0.20	2.50	1.25	1.23
Al$_2$O$_3$	33.25	33.07	32.61	34.51	34.17	32.62	35.01	34.60
FeO*	2.17	1.89	2.60	2.22	2.32	1.54	1.20	1.57
MnO	-	-	-	-	-	0.03	-	-
MgO	1.81	1.48	2.17	1.34	1.53	1.62	1.12	1.52
Na$_2$O	1.04	0.95	1.21	1.20	1.18	0.39	0.49	1.07
K$_2$O	9.77	9.81	9.73	9.64	9.57	10.82	10.86	9.84
Total	96.57	96.54	96.59	96.03	95.86	96.86	97.15	98.14

Cations on the basis of 22 oxygen atoms

Si	6.202	6.311	6.119	6.216	6.216	6.230	6.186	6.235
^{IV}Al	1.798	1.689	1.881	1.784	1.784	1.770	1.814	1.765
^{VI}Al	3.379	3.430	3.215	3.609	3.554	3.290	3.592	3.502
Ti	0.156	0.128	0.211	0.025	0.019	0.250	0.123	0.120
Fe	0.238	0.208	0.288	0.245	0.257	0.169	0.131	0.155
Mn	-	-	-	-	-	0.003	-	-
Mg	0.355	0.288	0.428	0.263	0.302	0.318	0.219	0.295
Na	0.265	0.249	0.311	0.306	0.303	0.102	0.125	0.264
K	1.648	1.642	1.645	1.631	1.618	1.817	1.814	1.814

Analysis 4: muscovite$_2$ replacing staurolite, 5: muscovite$_2$ replacing kyanite. (i) inclusion in garnet; FeO*: total iron as FeO. Compositions are expressed as wt% oxides.

TABLE 10. REPRESENTATIVE ELECTRON-MICROPROBE DATA ON BIOTITE FROM THE UPPER TECTONIC UNIT

	UER-16				UCR-7	UCR-5A	UER-1G
	1	2	3	4	5	6	7
SiO$_2$	37.32	36.43	37.21	35.86	35.72	36.45	39.20
TiO$_2$	1.82	1.89	2.60	0.96	1.33	1.45	1.12
Al$_2$O$_3$	19.84	21.06	18.82	19.36	21.17	19.14	18.36
FeO*	12.83	16.49	16.32	20.29	19.21	19.19	10.69
MnO	-	0.09	0.08	0.05	-	0.30	-
MgO	14.85	11.07	11.63	10.10	9.61	8.60	18.18
Na$_2$O	-	0.32	0.36	0.05	0.79	-	0.97
K$_2$O	10.20	9.68	9.66	10.00	9.40	10.09	8.64
Total	96.86	95.27	96.66	96.67	97.23	95.23	97.16

Cations on the basis of 22 oxygen atoms

Si	5.458	5.385	5.510	5.403	5.310	5.550	5.568
^{IV}Al	2.542	2.615	2.490	2.594	2.690	2.450	2.432
^{VI}Al	0.877	1.053	0.795	0.847	1.019	0.984	0.641
Ti	0.200	0.206	0.290	0.110	0.147	0.166	0.120
Fe	1.569	2.038	2.021	2.557	2.388	2.443	1.270
Mn	-	0.011	0.007	0.006	-	0.039	-
Mg	3.237	2.440	2.566	2.270	2.169	1.953	3.849
Na	-	0.093	0.104	0.015	0.228	-	0.266
K	1.903	1.823	1.824	1.924	1.783	1.959	1.566
X_{Mg}	0.67	0.54	0.56	0.47	0.48	0.44	0.75

Analyses 1 and 7: inclusion in garnet (biotite$_1$), 2: biotite$_2$ in contact with garnet, 4: biotite$_3$ (replacing garnet), 5: in contact with staurolite and kyanite, 6: in contact with staurolite and garnet. FeO*: total iron as FeO. Compositions are expressed in wt% oxides.

the large flakes of muscovite is their remarkably high Ti contents (up to 0.26 atoms p.f.u.) (Mposkos, unpubl. data). The highest content of Ti reported in the literature for muscovite is about 0.16 atoms p.f.u.; those values greater than 0.10 are from high-grade metamorphic rocks (Guidotti 1984, and references therein). The positive correlation of Ti with Mg + Fe and the negative

one with ^{VI}Al (Fig. 9) indicate that Ti in muscovite occupies octahedral sites, substituting for ^{VI}Al, according to the relation: $2(^{VI}Al^{3+}) = (^{VI}Ti^{4+}) + {}^{VI}(Mg + Fe^{2+})$, which is temperature-dependent ($\Delta V > 0$). The small flakes of retrograde muscovite contain negligible amounts of Ti.

Biotite

In the metapelites of "Type 2", biotite inclusions in garnet (biotite$_1$) are characterized by higher X_{Mg} values than the matrix biotite (biotite$_2$) (Table 10); the lowest X_{Mg} values were found in matrix biotite in contact with resorbed garnet or with garnet + kyanite$_2$. This finding agrees with observations of biotite formed at the expense of garnet (see below, reaction 11). The green to pale brown biotite that replaces garnet and muscovite (biotite$_3$, analysis 4) shows lower X_{Mg} values and remarkably lower Ti contents compared to the first and second generation of biotite (see also section on petrography). In the staurolite-bearing metapelites, biotite that coexists with staurolite and garnet is characterized by X_{Mg} values near 0.44 (analysis 6). This value is significantly lower than those of biotite from the metapelites lacking staurolite (X_{Mg} between 0.54 and 0.67). In the first case, biotite is formed, together with staurolite, at the expense of garnet (see below, reaction 8), as also suggested by the Fe-rich rim of the coexisting garnet and staurolite (see Table 7, anal. 6, Table 8, anal. 2).
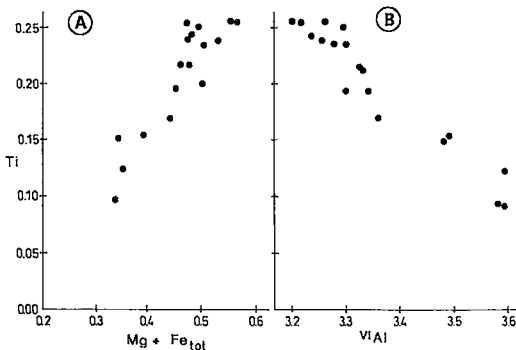

FIG. 9. Ti *versus* Mg + Fe$_{tot}$ (A) and Ti *versus* ^{VI}Al (B) plot of potassic white mica from a representative sample (UWR–8E) of the pelitic rocks of the UTU. A positive correlation between Ti and Mg + Fe$_{tot}$ and a negative correlation between Ti and ^{VI}Al is observed (also see text).

The grain of phlogopite which, together with garnet, was found in a kyanite inclusion within one garnet porphyroblast exhibits X_{Mg} values on the order of 0.75 (anal. 7).

Chlorite

In the UTU, chlorite was found only in the first type of metapelites, characterized by mineral assemblage (a). It appears both as inclusion in garnet and in the rock matrix. The two types of chlorite differ chemically; the inclusions in garnet are characterized by a higher X_{Mg} value (0.75, analysis 1 of Table 11) compared to chlorite in the matrix (0.66–0.69) in the same sample. The inclusions of chlorite in garnet have ^{IV}Al greater than ^{VI}Al, which indicates that part of the iron is in the trivalent state. The matrix chlorite evidently lacks ferric iron, because it has ^{IV}Al less than ^{VI}Al. Al_{tot} of chlorite in the inclusions ranges between 5.089 and 5.229 atoms p.f.u., whereas Al_{tot} of chlorite in the matrix varies between 5.262 and 5.411. This suggests a higher proportion of the Tschermak substitution in the latter type of chlorite. The presence of ferric iron in chlorite of the inclusions and its higher X_{Mg} value and lower extent of Tschermak substitution suggest higher-pressure conditions of formation compared to matrix chlorite (Chopin 1979, Powell & Holland 1990).

Petrological interpretation of the textural and mineral chemical data

The textural observations, in conjunction with the mineral chemical data, suggest an evolution of the mineral assemblages in both types of metapelites following a sequence of reactions that have taken place.

In metapelites of "Type 1" characterized by mineral assemblage (a), the presence of Ky + Chl + Ms and of Ky + Phl inclusions in garnet porphyroblasts indicates that during prograde metamorphism, growth of garnet took place under P–T conditions above the upper stability limit of staurolite (cf. Fig. 11B, below). The staurolite of the matrix in these rocks is therefore a product of a later, retrograde stage of metamorphism related to exhumation of the UTU. As is indicated by the close association of staurolite with kyanite (resorbed grains of kyanite enclosed in staurolite; see "Petrography"), the formation of staurolite in this type of metapelites can be ascribed to the retrograde reaction:

$$Grt + Ky + H_2O = St + Qtz \qquad (5)$$
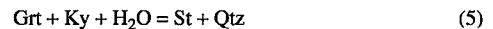
The chemical composition of the AFM phases (decrease of the X_{Mg} value in garnet and staurolite from core to rim; Table 7, analyses 7 and 8, and Table 8, analyses 5 and 6, respectively) provides additional evidence in favor of this view. Where staurolite coexists with garnet and chlorite, its formation may be related to the retrograde reaction:

$$Grt + H_2O = St + Chl + Qtz \qquad (6)$$

According to Thompson (1976, p. 416), reaction (6) takes place at lower metamorphic grades than reaction (5). This proves true in the above described metapelites, in which the chemical composition of staurolite resulting by reaction (6) is characterized by lower X_{Mg} values (0.21, analysis 8 of Table 8) compared to the staurolite participating in reaction (5) (0.29, analysis 6 of Table 8) in the same sample. Chlorite coexisting with staurolite also is characterized by lower X_{Mg} values (0.66, analysis 3, Table 11) than that enclosed in garnet (0.75, analysis 1, Table 11), indicating its retrograde derivation.

In metapelites of "Type 1" with mineral assemblage (b), information on the prograde stage of metamorphism is provided by the presence of mineral inclusions in garnet (samples UCR–5C, UCR–6 and UCR–7). The presence of ilmenite and of staurolite with ilmenite inclusions in the core of the garnet crystals and of rutile only toward the outer part of the same garnet (sample UCR–5; Fig. 6C) indicates that growth of garnet took place with increasing pressure, according to the pressure-dependent reaction:

$$St + Ilm + Qtz = Alm + Rt + H_2O \qquad (7)$$
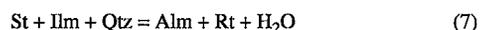
(Ballèvre et al. 1989). P–T conditions during garnet

TABLE 11. REPRESENTATIVE ELECTRON-MICROPROBE DATA ON CHLORITE FROM THE UPPER TECTONIC UNIT

	UER-1G		
	1	2	3
SiO₂ wt%	26.81	27.85	26.10
TiO₂	0.11	--	--
Al₂O₃	21.59	22.22	21.74
FeO*	14.77	16.17	18.24
MnO	--	--	--
MgO	23.44	20.08	19.79
Na₂O	0.77	0.49	0.71
Total	87.49	87.28	86.58

Cations on the basis of 28 oxygen atoms

|			
Si	5.362	5.615	5.370
^{IV}Al	2.638	2.383	2.630
^{VI}Al	2.451	2.876	2.642
Ti	0.016	--	--
Fe	2.471	2.718	3.139
Mn	--	--	--
Mg	6.988	6.014	6.070
Na	0.298	0.192	0.283
X_{Mg}	0.75	0.69	0.66

Analyses 1: inclusion in garnet (chlorite₁), 2, 3: matrix chlorite (chlorite₂). FeO*: total iron as FeO.

growth probably exceeded the upper stability limit of staurolite (*cf.* Fig. 11B, below), as indicated by the presence of kyanite + biotite inclusions in garnet of samples UCR–6 and UCR–7. The formation of matrix staurolite in metapelites with mineral assemblage (b) is therefore related to the retrograde stage of metamorphism.

The pattern of zonation in the garnet inclusions in staurolite$_2$ (Fig. 8B), observed in samples UCR–5A, UCR–5C and UER–3, which exhibits a decrease in Mg and increase in Fe, Mn in the outermost rim, suggests that staurolite growth is possibly a result of the retrograde reaction:

$$Grt + Ms + H_2O = St + Bt + Qtz \qquad (8)$$

In samples UCR–6 and UCR–7, the replacement of kyanite by staurolite (Fig. 6E) took place according to the retrograde reaction:

$$Ky + Bt + H_2O = St + Ms + Qtz \qquad (9)$$
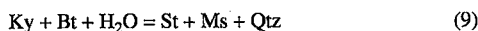
Replacement of staurolite by sillimanite (Fig. 6F) in the same samples is probably related to the prograde reaction:

$$St + Ms + Qtz = Sil + Bt + H_2O \qquad (10)$$
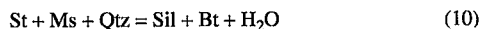
In metapelites of "Type 2" prograde metamorphic conditions are inferred by the presence of kyanite$_1$, biotite, muscovite, and plagioclase inclusions within garnet porphyroblasts. The paragenesis Grt + Ky$_1$ + Bt + Ms + Qtz + Pl, which is observed also in the matrix, suggests that conditions of metamorphism were above the upper stability limit of staurolite (Fig. 11B).

A number of reactions that took place in this type of metapelite during exhumation is inferred by the inverse pattern of zoning in garnet, demonstrated in the outermost rim (Fig. 8A, C) by the lower X_{Mg} values of matrix biotite in comparison with that enclosed in garnet (Table 10), as well as by textural characteristics. Replacement of garnet by biotite + kyanite$_2$ is attributed to the pressure-dependent reaction:
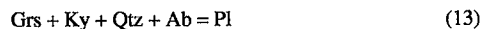
$$Grt + Ms = Ky + Bt + Qtz \qquad (11)$$

In the case that garnet is replaced by biotite + plagioclase, the reaction

$$Grt + Ms + Pl = Bt + Ca\text{-richer Pl} \qquad (12)$$
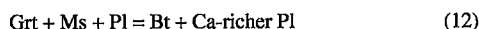
should have taken place.

Textural relationships of plagioclase (see Petrography) indicate that plagioclase was formed at the expense of Grt + Ky + Qtz + Ab, according to a reaction of the type

$$Grs + Ky + Qtz + Ab = Pl \qquad (13)$$

probably during decompression.

Sillimanite in this type of metapelite does not form by replacement of kyanite but is related to more complex reactions. In the case where "fibrolite" associated with biotite and muscovite occurs as felted masses around garnet crystals (Fig. 7B), its formation is possibly related to the reaction

$$Grt + Ms = Bt + Sil + Qtz \qquad (14)$$
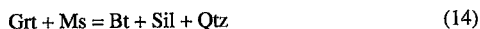
The chemical zoning of garnet, which shows a significant increase in Mn and decrease in X_{Mg} value only in the outermost rim (see zoning pattern of Fig. 8A) reinforces the view that sillimanite formation is related to reaction (14). The sillimanite masses within muscovite and biotite probably reflect more complex reactions involving primary phengite and plagioclase.

The presence of numerous inclusions of sagenitic rutile in large flakes of muscovite suggests the pre-existence of biotite. "Sagenite"-bearing muscovite is reported from high-pressure metapelites (*e.g.*, Sesia zone, western Alps; Vuichard & Ballèvre 1988) and is interpreted to have been derived from earlier-formed biotite. Small flakes of biotite at the borders of large grains of muscovite oriented along the cleavage (see, for instance, large grain of muscovite at the bottom of Fig. 6E) may be related to the decomposition of the celadonite component of earlier-formed phengite.

The absence of muscovite and the presence of K-feldspar + sillimanite in this type of metapelite, which occurs mainly in the area south of Thermes, central Rhodope (samples UCR–19 and UCR–19A; Fig. 1B) indicate that the highest metamorphic grade of the Upper Tectonic Unit was reached in this area.

PHASE RELATIONS

AFM topologies for the metapelites of the UTU were projected following the same procedure as for the LTU (see p. 408). The mineral parageneses of the metapelites are graphically illustrated in a sequence of AFM diagrams (Figs. 10A–10G). Figures 10A, B, C correspond to successive steps of the prograde stage; the compositions depicted represent minerals found as inclusions in garnet porphyroblasts. In the three-phase assemblage Ky – Grt – St (A), staurolite occurs as inclusion in a garnet grain that shows an increase in X_{Mg} in its outermost rim. Staurolite inclusions in the garnet rim have a greater X_{Mg} than those enclosed in the core. Figures 10B and 10C refer to the three-phase assemblages Ky – Grt – Chl and Ky – Grt – Phl, respectively.

The successive steps of the exhumation stage are represented by Figures 10D, E, F and G. In (D), matrix staurolite, which grew at the expense of kyanite + garnet (reaction 5), shows a decrease in X_{Mg} from core to rim. The composition of the garnet rim that takes part in the above reaction is poorer in Mg compared to the core. Matrix staurolite and chlorite form at the expense of
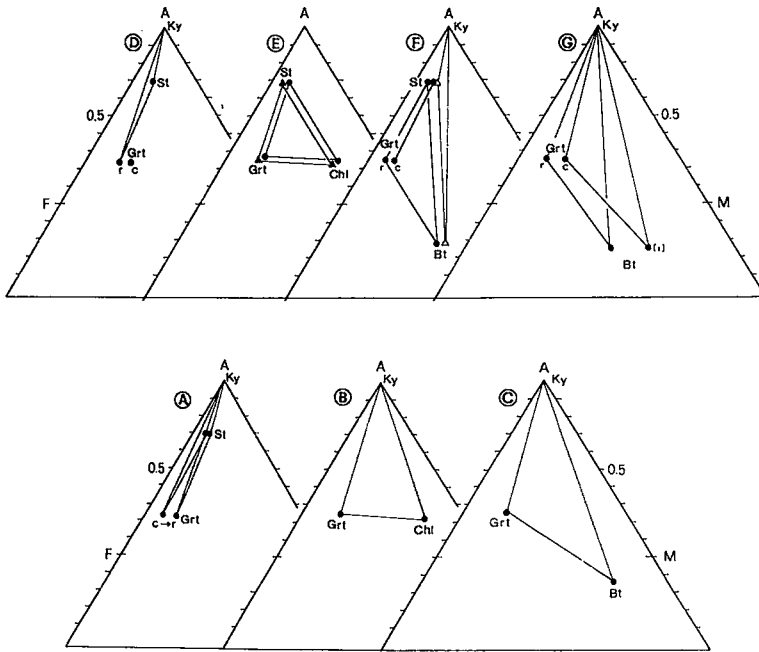
FIG. 10. AFM projections of assemblages that coexist with potassic white mica – quartz – rutile ± ilmenite – H$_2$O in the pelitic rocks of the UTU. Diagrams (A), (B) and (C) correspond to successive steps of the prograde stage. The projected mineral phases are inclusions in garnet. Diagrams (D), (E), (F) and (G) correspond to successive steps of the exhumation stage. In diagram (E), triangles and circles correspond to two analyzed parageneses from the same sample.

garnet (reaction 6). A decrease in X_{Mg} of the reacting phases also is observed (Fig. 10E), which indicates the retrograde character of reaction (6). In metapelites of "Type 1" with mineral assemblage (b) (Fig. 10F), staurolite forms from kyanite + biotite (reaction 9) (sample UCR–7) or from garnet + muscovite (reaction 8) (sample UCR–5A). The phases participating in reaction (8) show progressive Fe-enrichment from core to rim (see garnet and staurolite in F). In metapelites of "Type 2" (G), the association biotite + kyanite$_2$ is produced from garnet + muscovite (reaction 11), and the compositions of the outer part of the reacting garnet and of biotite are remarkably poorer in Mg than garnet cores and biotite inclusions in garnet.

METAMORPHIC EVOLUTION

All the P–T data and constraints discussed above are combined into a single diagram for each tectonic unit (Figs. 11A, B) for P(H$_2$O) = P$_{total}$. Multivariant mineral reactions, inferred from the textural relationships and the mineral chemical data, were calculated with the GEØ–CALC software (Brown et al. 1988) using the database of Berman (1988). Univariant reactions that define the

stability field of staurolite were taken from the KFMASH petrogenetic grid of Vuichard & Ballèvre (1988). The resulting P–T path for the metapelites was completed with data for the associated eclogites.

Prograde path and peak conditions of metamorphism of the Lower Tectonic Unit

Critical mineral or textural indicators with which to construct the prograde path of the LTU are not present in the metapelites. Glaucophane inclusions in garnet of the eclogites of eastern Rhodope (Mposkos, unpubl. data), as well as from the Bulgarian part of Rhodope (Burg, pers. comm., 1991) indicate that during burial, the stability field of glaucophane was crossed.

The high-pressure paragenesis Grt + Cld + Chl + Phen is widespread in the metapelites of "Type 1". The paragenesis Grt + Cld + Chl is stable in a broad range of pressure (between 4 and 18 kbar). However, geobarometry applied to coexisting phengite with the highest Si content (6.87) yielded, according to Massonne & Schreyer (1987), pressures of 13–13.5 kbar (for temperatures corresponding to between 550° and 600°C, as reported from the adjacent eclogites: Liati & Mposkos
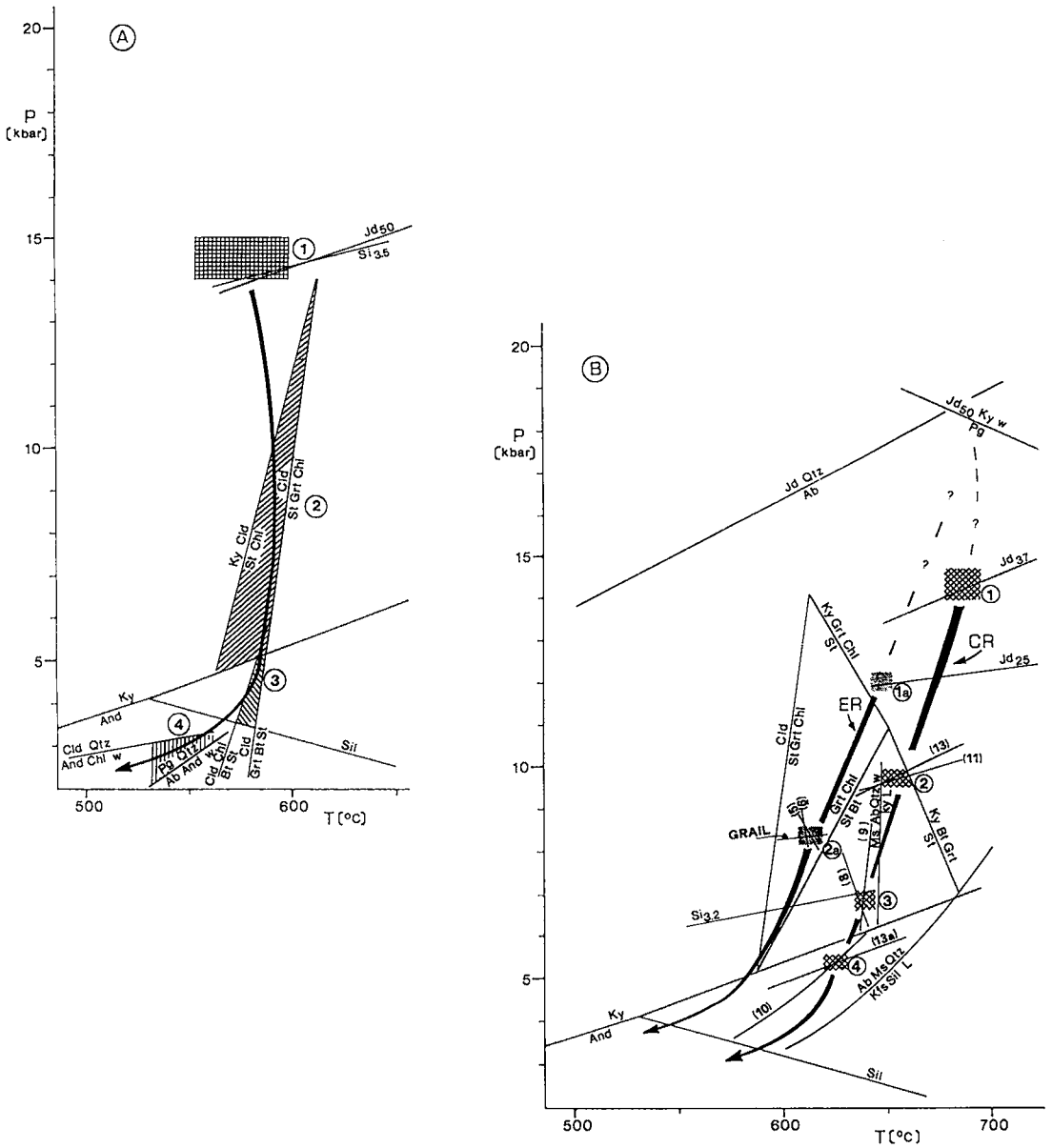
FIG. 11. Estimated P–T conditions of intermediate steps of the exhumation and tentative reconstruction of the P–T paths for the lower (A) and upper tectonic unit (B) of Rhodope. Peak metamorphic conditions are marked only for the LTU. A. Cross-hatched field corresponds to peak P–T conditions. The $Si_{3.5}$ isopleth is from Massonne & Schreyer (1987); the Jd_{50} isopleth is from Gasparik & Lindsley (1981). The triple point for the aluminosilicates is from Bohlen et al. (1991). The curve Cld + Qtz = And + Chl + w was obtained with the GEØ–CALC software (Brown et al. 1988). The curve Pg + Qtz = Ab + And + w is from Chatterjee (1972). All other curves are from the petrogenetic grid of the KFMASH system (taken from Vuichard & Ballèvre 1988). B. Cross-hatched field 1 and shaded field 1a correspond to the highest known P–T conditions for the UTU of central (CR) and eastern (ER) part of Rhodope. Fields 2, 3, 4 and 2a correspond to the estimated P–T conditions of intermediate steps of the exhumation. Dashed lines are probable extrapolations of the exhumation paths from higher pressures. The stability field of staurolite (reaction curves from the petrogenetic grid of Vuichard & Ballèvre 1988) is outlined. The curve Pg = Jd_{50} + Ky + w is from Holland (1979). The GRAIL geobarometer is from Bohlen et al. (1983). Curves (5), (6), (8), (9), (10), (11), (13) and (13a) (see text for the corresponding reactions) were obtained with the GEØ–CALC software (Brown et al. 1981) and the database of Berman et al. (1988), calculated with the analyzed composition of coexisting mineral phases.

1990). The resulting pressures are minimum values because phengite is not in the appropriate paragenesis required for the application of the above geobarometer (see Massonne & Schreyer 1987). Nevertheless, similar conditions of pressure (14–15 kbar; field 1 in Fig. 11A) are reported for the adjacent quartzofeldspathic rocks, where phengite does coexist with the limiting assemblage quartz + albite + microcline + biotite (Mposkos 1989a). P–T conditions of 15 kbar and 550°–600°C also are reported for associated eclogites (Liati & Mposkos 1990).

Exhumation path of the Lower Tectonic Unit

The various stages of the exhumation path are well recorded in a single sample of "Type 1" metapelite having the mineral assemblage (b) (Grt – Cld – St – Chl – Phen/Ms – Pg – Bt – Ky – And – Qtz – Rt – Ilm; Table 1) (*i.e.*, samples LER–8B, LER–8C, LER–8D). The early portion of the exhumation path is reflected in the decomposition of chloritoid to staurolite. Persistence of the paragenesis Cld – St – Chl (AFM diagram B in Fig. 5) confines the exhumation trajectory to the field between the curves Ky + Cld = St + Chl and Cld = St + Chl + Grt (Fig. 11A, field 2). Replacement of chloritoid by staurolite + biotite and persistence of Cld – St – Bt suggest that the trajectory should enter the narrow field defined by the curves Cld + Chl = Bt + St and Cld = Grt + Bt + St (Fig. 11A, field 3). The formation of andalusite + chlorite$_3$ at the expense of chloritoid (reaction 3) at still lower pressures allows the P–T trajectory to enter the field of stability of andalusite (Fig. 11A, field 4) and to pass above the decomposition curve of paragonite + quartz, because paragonite remains stable in these rocks. Replacement of chloritoid by Fe-rich chlorite (chlorite$_3$) in the same rocks is related to this stage of the exhumation. The absence of staurolite from the garnet – chloritoid schists, located in the southeastern part of eastern Rhodope and in western Rhodope, is attributed to the fact that these rocks followed a path of exhumation outside the field of stability of Cld – St – Chl (see Fig. 11A and Mposkos 1989a for details). The complete path of exhumation shown in Figure 11A for the LTU implies that initial uplift occurred along a nearly isothermal path. A slight increase in temperature during the medium-pressure overprint is reflected in the growth of hornblende around tremolite in the metabasites and of oligoclase around albite in gneisses, metapelites and metabasic rocks (Mposkos 1989a,b, Liati & Mposkos 1990). Significant cooling did not occur until the rocks were within ~12 km of the surface.

Prograde path and peak conditions of metamorphism of the Upper Tectonic Unit

In the Upper Tectonic Unit, mineral phases that occur as inclusions in garnet can provide some information about the assemblages that were stable prior to peak conditions of metamorphism. The first constraints for the prograde path are provided by staurolite inclusions in garnet porphyroblasts (sample UCR–5C). This staurolite is characterized by X_{Mg} values higher than those of the host garnet (Tables 7, 8), indicating that the prograde trajectory crossed the stability field of staurolite below 14.5 kbar, at which pressure inverse Fe–Mg partitioning between staurolite and garnet appears (Vuichard & Ballèvre 1988). The presence of staurolite + rutile inclusions in garnet rims sets a minimum pressure limit of 11 kbar for the prograde path (Ballèvre *et al.* 1989). At higher pressures, the prograde trajectory enters the stability field of kyanite + chlorite + muscovite inclusions within garnet porphyroblasts (samples UER–1A, UER–1G and UER–2, eastern Rhodope). It is noted that the paragenesis Grt – Ky – Chl is stable at pressures between 11 and 17 kbar, at temperatures of 610°–650°C, according to Vuichard & Ballèvre (1988), or between 13 and 16 kbar, according to Mottana *et al.* (1990), above the stability field of staurolite.

The peak conditions of the high-pressure metamorphism are uncertain. Extensive overprinting metamorphism of high-grade rocks has obliterated the primary assemblages. The mineral association garnet + kyanite + biotite, which is widespread in the pelitic rocks of the UTU, both in the matrix and as kyanite + biotite inclusions in garnet, appears to partially represent the high-pressure paragenesis. However, this paragenesis has a wide field of stability and is not diagnostic of high pressures. The presence of plagioclase and the lack of jadeite as inclusions in garnet suggest an upper limit in pressure defined by the reaction Ab = Jd + Qtz. The coexistence of omphacite (Jd$_{50}$) + kyanite in eclogites of central Rhodope near the Greek-Bulgarian borders (Ardino area) implies, according to the reaction Pg = Jd$_{50}$ + Ky + H$_2$O (Holland 1979), pressures in excess of 18 kbar, provided that a(H$_2$O) was equal to unity (Liati & Mposkos 1990). Note that a(H$_2$O) below unity significantly lowers the equilibrium pressure of the above reaction.

Exhumation path of the Upper Tectonic Unit

The starting point for the exhumation path is provided by thermobarometric calculations for partly amphibolitized eclogites of central (670°–690°C, 14 kbar; field 1) and eastern Rhodope (640°–660°C, 12 kbar; field 1a) (unpublished data by the authors). Note that the amphibolitized eclogitic rocks are concordantly interlayered within the metapelites studied; both rock types were involved in the same metamorphic history. Intermediate P–T steps during continuous unloading were obtained by reactions that remained incomplete, as indicated by the preservation of replacement textures in the metapelitic rocks studied.

Information on the P–T conditions of the next stage of the uplift in central Rhodope and partly in eastern

Rhodope is provided by metapelites of "Type 2" (samples UCR–12, UCR–13, UER–16, UER–17), in which the assumed high-pressure mineral association was garnet + kyanite + biotite + phengite + Na-rich plagioclase + quartz + rutile. The presence of kyanite-bearing neosomes suggests that exhumation proceeded above the melting reaction: Ms + Ab + Qtz + w = Ky + L (Thompson & Algor 1977). The existence of Na-rich plagioclase in the primary high-pressure assemblage is inferred from kyanite + quartz + plagioclase inclusions in garnet; kyanite + quartz + garnet are replaced by plagioclase, according to a reaction like (13). Gt – Pl – Ky – Qtz geobarometry (according to Ganguly & Saxena 1984) applied to Pl + Ky + Qtz inclusions in garnet yielded pressures between 9 and 11 kbar; slightly lower pressures were obtained from matrix plagioclase. Temperature conditions above the melting curve Ms + Ab + Qtz + w = Ky + L and below the curve St = Ky + Bt + Grt, combined with the results of geobarometry (curve 13), define field (2) (Fig. 11B), which should have been crossed during further unroofing. Although these metapelites lack staurolite, apparently as a result of an unsuitable bulk composition, its presence in concordantly interlayered metapelites located in the immediate vicinity suggests that metamorphic conditions were within the stability field of this mineral. Moreover, reaction (11), which proceeds in the direction of decompression and produces Ky_2 + Bt from Grt + Ms, occurs in field (2) and is therefore related to that stage of the uplift.

Information on the next steps of the path of exhumation is obtained from the metapelites of "Type 1" (samples UCR–5A, UCR–5C, UCR–6, central Rhodope), in which the high-pressure mineral association was probably garnet + kyanite + phengite + biotite + quartz + rutile. In these rocks, staurolite is formed at the expense of kyanite + biotite (reaction 9) and of garnet + muscovite (reaction 8). Intersection of these two reaction curves with the isopleth $Si_{3.2}$ of coexisting potassic white mica defines reference field (3) in Figure 11B. In the same rocks, sillimanite forms partly at the expense of staurolite according to reaction (10), providing additional information for the portion of the exhumation path lying at slightly lower pressures. These pressures were estimated by Pl – Grt – Sil – Qtz geobarometry (sample UCR–14) (curve 13a) which, combined with reaction curve (10), defines field (4) in Figure 11B. The path of uplift probably entered the field of stability of andalusite (replacement of kyanite by andalusite; see "Petrography") and proceeded with a very smooth slope with respect to the temperature axis until the unit reached the surface. In the area of Thermes, the reaction curve Ab + Ms + Qtz = Kfs + Sil + L must have been crossed, as indicated by petrographic data (Kfs + Sil instead of muscovite, sample UCR–19). To achieve the temperatures required for Kfs + Sil to appear, a local high heat-flow during the late evolution of Rhodope is suggested. Late Eocene, syntectonic magmatism (e.g.,

Kentavros monzodiorite, south of Thermes dated at 38 Ma; Liati & Kreuzer 1990) could explain increased heat-flow in this area.

In the easternmost part of Rhodope, exhumation in the Upper Tectonic Unit seems to have followed a different trajectory compared to that in central Rhodope. This is indicated by the succession of mineral assemblages in the metapelites containing Grt – Ky – St – Chl – Ms – Qtz – Rt ± Ilm (samples UER–1A, UER–1G, UER–2). In these metapelites, the high-pressure mineral assemblage was probably Grt – Ky – Phen – Chl – Phl – Qtz – Rt. Metamorphism during decompression is recorded in these rocks by the growth of matrix staurolite at the expense of kyanite + garnet (retrograde reaction 5) and, at lower temperatures (Thompson 1976), by the formation of staurolite + chlorite at the expense of garnet (retrograde reaction 6). Both reactions (5) and (6) occur within the stability field of staurolite, on the left side of the reaction curve Grt + Chl = St + Bt. Intersection of these reactions with the curve corresponding to the GRAIL geobarometer (Bohlen et al. 1983) applied to the garnet – rutile – ilmenite assemblage of the same sample defines the reference field (2a) (Fig. 11B), which should have been crossed during uplift. In view of the absence of biotite and persistence of the paragenesis St + Grt + Chl, the P–T trajectory proceeded on the left side of the reaction Grt + Chl = St + Bt, inside this field. The shape of the trajectory constructed on the basis of the above data suggests that exhumation in the easternmost part of Rhodope proceeded along a path lying at temperatures of about 30°C lower than those defined for central Rhodope. It is therefore possible that this part of the Upper Tectonic Unit of Rhodope constitutes the uppermost parts of the rock sequence, which were buried at shallower depths during prograde metamorphism and followed a path of exhumation characterized by a lower grade. Another possibility could be that a tectonic discontinuity exists in this part of the Upper Tectonic Unit.

The low-pressure, greenschist-facies stage of the exhumation is marked both in central and eastern Rhodope by the widespread alteration of garnet to green biotite ($biotite_3$) and chlorite, by sericitization of kyanite and staurolite, and by replacement of kyanite by andalusite. The replacement of kyanite by andalusite is rarely observed (i.e., sample UER–4 of eastern Rhodope).

DISCUSSION

Most thermal models of thickened crust (England & Richardson 1977, Draper & Bone 1981, England & Thompson 1984) show P–T paths characterized by significant heating after the maximum pressure. In contrast, the P–T path relevant to Rhodope, constructed on the basis of our petrological investigation of metapelites and complemented with data from concordantly intercalated orthogneisses and amphibolitized eclogites,

reflects a coincidence of peak pressure and peak temperature during metamorphic evolution. In the LTU, maximum P–T conditions are 550°–600°C and 14–15 kbar (Mposkos 1989a, Liati & Mposkos 1990). Exhumation was nearly isothermal to a depth of about 12 km from the surface and continued along a trajectory characterized by significant cooling. In the UTU, although precise peak conditions of metamorphism are uncertain, the highest pressures are assumed to have reached at least 18 kbar, indicating that this unit was buried at greater depths than the LTU. Exhumation was characterized by cooling; the rocks spent a large part of their ascent history within a small range of temperature from the highest known temperatures, and finally proceeded along a trajectory reflecting high rates of cooling, until they reached the surface.

The discrepancies identified in the form of the exhumation paths of the two tectonic units (cf. Figs. 11A, B) reflect their relative position during unloading. The UTU, which reached greater depths in the prograde part of metamorphism, was thrust over the LTU in the exhumation stage. The overthrust took place at depth, under conditions of ductile deformation, so that the discontinuity between the two tectonic units can only be determined on petrological grounds. Therefore, the UTU acted as a warm slab that prevented the rocks of the LTU from losing heat for a long duration of the exhumation history. The relative lack of thermal overprint during exhumation may be attributed to rapid uplift and limited transfer of heat from the mantle.

Similar exhumation paths to that of the Rhodope have been proposed also for other high-pressure terranes, i.e., Western Alps (Sesia zone; Rubie 1984, Briançonnais zone; Goffé & Velde 1984), the Seward Peninsula, northern Alaska (Patrick & Evans 1989), the Cyclades in the Aegean Sea (Matthews & Schliestedt 1984, Schliestedt 1986, Avigad & Garfunkel 1991). The cooling, which accompanied exhumation in the Alps, was postulated to be a result of continuous underthrusting of cold material below the accretionary wedge, where high-pressure rocks emerged (Goffé & Velde 1984, Rubie 1984, Goffé & Chopin 1986). For the area of the Cyclades, underthrusting of external units has been suggested by Altherr et al. (1982), whereas Avigad & Garfunkel (1991) proposed that the cooling of the Cycladic rocks was a result of the rapid unroofing tectonics rather than of the continuous underthrusting. In the Rhodope zone, the problem of the mechanism by which the high-pressure rocks returned to the surface remains poorly understood. The recognition of a complex nappe structure (Ivanov 1988, Burg et al. 1990, Koukouvelas & Doutsos 1990) indicates that tectonic processes predominated. Since the P–T path of the Rhodope terrane shows important similarities in form with that of the southerly lying high-pressure belt of the Cyclades, analogous constraints (rapid unroofing tectonics or continuous underthrusting of cold material) can be invoked.

REFERENCES

ALTHERR, R., KREUZER, H., WENDT, I., LENZ, H., WAGNER, G.A., KELLER, J., HARRE, W. & HOHNDORF, A. (1982): A late Oligocene/early Miocene high temperature belt in the Attic-Cycladic crystalline complex (SE Pelagonia, Greece). Geol. Jahrb. E23, 97-164.

ARNAUDOV, V., AMOV, B., CHERNEVA, Z., ARNAUDOVA, R., PAVLOVA, M. & BARTITSKY, E. (1990): Petrological–geochemical and lead isotope evidence of Alpine metamorphism in the Rhodope crystalline complex. Geol. Balc. 20(5), 29-44.

AVIGAD, D. & GARFUNKEL, Z. (1991): Uplift and exhumation of high-pressure metamorphic terrains: the example of the Cycladic blueschist belt (Aegean Sea). Tectonophys. 188, 357-372.

BALLÈVRE, M., PINARDON, J.L., KIENAST, J.-R. & VUICHARD, J.P. (1989): Reversal of Fe–Mg partitioning between garnet and staurolite in eclogite-facies metapelites from the Champtoceaux nappe (Brittany, France). J. Petrol. 30, 1321-1349.

BERMAN, R.G. (1988): Internally consistent thermodynamic data for minerals in the system $Na_2O–K_2O–CaO–MgO–FeO–Fe_2O_3–Al_2O_3–SiO_2–TiO_2–H_2O–CO_2$. J. Petrol. 29, 445-522.

BOHLEN, S.R., MONTANA, A. & KERRICK, D.M. (1991): Precise determinations of the equilibria kyanite–sillimanite and kyanite–andalusite and a revised triple point for Al_2SiO_5 polymorphs. Am. Mineral. 76, 677-680.

————, WALL, V.J. & BOETTCHER, A.L. (1983): Experimental investigations and geological applications of equilibria in the system $FeO–TiO_2–Al_2O_3–SiO_2–H_2O$. Am. Mineral. 68, 1049-1058.

BROWN, T.H., BERMAN, R.G. & PERKINS, E.H. (1988): GEØ–CALC: software for calculation and display of pressure-temperature-composition phase diagrams using an IBM or compatible personal computer. Comput. & Geosci. 14, 279-289.

BURCHFIEL, B.C. (1980): Eastern European Alpine system and the Carpathian orocline as an example of collision tectonics. Tectonophys. 63, 31-61.

BURG, J.-P., IVANOV, Z., RICOU, L.-E., DIMOR, D. & KLAIN, L. (1990): Implications of shear-sense criteria for the tectonic evolution of the Central Rhodope massif, southern Bulgaria. Geology 18, 451-454.

CHATTERJEE, N.D. (1972): The upper stability limit of the assemblage paragonite + quartz and its natural occurrences. *Contrib. Mineral. Petrol.* **34**, 288-303.

CHOPIN, C. (1979): *De la Vanoise au Grand Paradis: une approche pétrographique et radiochronologique de la signification géodynamique du métamorphisme de haute pression.* Thèse 3$^{\text{ième}}$ cycle, Université de Paris VI, Paris, France.

_____, HENRY, C. & MICHARD, A. (1991): Geology and petrology of the coesite-bearing terrain, Dora Maira massif, Western Alps. *Eur. J. Mineral.* **3**, 263-291.

_____ & MALUSKI, H. (1980): ^{40}Ar–^{39}Ar dating of high-pressure metamorphic micas from the Gran Paradiso Area (Western Alps): evidence against the blocking temperature concept. *Contrib. Mineral. Petrol.* **74**, 109-122.

_____ & SCHREYER, W. (1983): Magnesiocarpholite and magnesio-chloritoid: two index minerals of pelitic blueschists in the model system MgO–Al$_2$O$_3$–SiO$_2$–H$_2$O. *Am. J. Sci.* **283A**, 72-96.

CIMMINO, F. & MESSIGA, B. (1979): I calcescisti del Gruppo di Voltri (Liguria Occidentale) le variationi compositionali delle miche bianche in rapporto alla evoluzione tettonico-metamorphica alpina. *Ofioliti* 4(3), 269-294.

DÉLOR, C., BURG, J.-P., GUIRAUD, M. & LEYRELOUP, A. (1987): Les métapélites à phengite-chloritoïde-grenat-staurotide-disthène de la klippe de Najac-Carmaux: nouveaux marqueurs d'un métamorphisme de haute pression varisque en Rouergue occidentale. *C.R. Acad. Sci. Paris* **305**, (II), 589-595.

DEMPSTER, T.J. (1992): Zoning and recrystallization of phengitic micas: implications for metamorphic equilibration. *Contrib. Mineral. Petrol.* **109**, 526-537.

DRAPER, G. & BONE, R. (1981): Denudation rates, thermal evolution and preservation of blueschist terrains. *J. Geol.* **89**, 601-613.

ENGLAND, P. & RICHARDSON, S.W. (1977): The influence of erosion upon the mineral facies of rocks from different metamorphic environments. *J. Geol. Soc. London* **134**, 201-213.

_____ & THOMPSON, A.B. (1984): Pressure-temperature-time paths of regional metamorphism. I. Heat transfer during the evolution of regions of thickened continental crust. *J. Petrol.* **25**, 894-928.

EVANS, B.W. & PATRICK, B.E. (1987): Phengite-3T in high-pressure metamorphosed granitic orthogneisses, Seward Peninsula, Alaska. *Can. Mineral.* **25**, 141-158.

FRANZ, G., THOMAS, S. & SMITH, D.C. (1986): High-pressure phengite decomposition in the Weissenstein eclogite, Münchberg Gneiss Massif, Germany. *Contrib. Mineral. Petrol.* **92**, 71-87.

GANGULY, J. & SAXENA, S.K. (1984): Mixing properties of alumino-silicate garnets: constraints from natural and experimental data, and applications to geothermo-barometry. *Am. Mineral.* **69**, 88-97.

GASPARIK, T. & LINDSLEY, H. (1981): Phase equilibria at high pressures of pyroxenes containing monovalent and trivalent ions. *In* Pyroxenes (C.T. Prewitt, ed.). *Rev. Mineral.* **7**, 309-339.

GHENT, E.D., STOUT, M.Z., BLACK, P.M. & BROTHERS, R.N. (1987): Chloritoid-bearing rocks associated with blueschists and eclogites, northern New Caledonia. *J. Metamorph. Geol.* **5**, 239-254.

GOFFÉ, B. & CHOPIN, C. (1986): High-pressure metamorphism in the western Alps: zoneography of metapelites, chronology and consequences. *Schweiz. Mineral. Petrogr. Mitt.* **66**, 41-52.

_____ & VELDE, B. (1984): Contrasted metamorphic evolutions in thrusted cover units of the Briançonnais zone (French Alps): a model for the conservation of HP–LT metamorphic mineral assemblages. *Earth Planet. Sci. Lett.* **68**, 351-360.

GUIDOTTI, C.V. (1984): Micas in metamorphic rocks. *In* Micas (S.W. Bailey, ed.). *Rev. Mineral.* **13**, 357-468.

HEINRICH, C.A. (1982): Kyanite–eclogite to amphibolite facies evolution of hydrous mafic and pelitic rocks, Adula Nappe, central Alps. *Contrib. Mineral. Petrol.* **81**, 30-38.

HOLLAND, T.J.B. (1979): Experimental determination of the reaction: paragonite = jadeite + kyanite + H$_2$O, with applications to eclogites and blueschists. *Contrib. Mineral. Petrol.* **68**, 293-301.

IVANOV, Z. (1988): Aperçu générale sur l'évolution géologique et structurale du massif des Rhodopes dans le cadre des Balkanides. *Bull. Soc. géol. France* **8**, t. IV(2), 227-240.

KOCKEL, F. & WALTHER, H.W. (1965): Die Strimon Linie als Grenze zwischen Serbo-Mazedonischem und Rila-Rhodope Massiv in Ost Mazedonien. *Geol. Jahrb.*, 575-602.

KOLCEVA, K., ZELJAZKOVA-PANAJOTOVA, M., BOBRECOV, N.L. & STOJANOVA, V. (1986): Eclogites in Central Rhodope metamorphic group and their retrograde metamorphism. *Geochem. Mineral. and Petrol. (Sofia)* **20/21**, 130-144.

KOUKOUVELAS, J. & DOUTSOS, T. (1990): Tectonic stages along a traverse cross cutting the Rhodopian zone (Greece). *Geol. Rundsch.* **79**(3), 753-776.

KRETZ, R. (1983): Symbols for rock-forming minerals. *Am. Mineral.* **68**, 277-279.

LIATI, A. (1986): *Regional Metamorphism and Overprinting Contact Metamorphism of the Rhodope Zone, near Xanthi, N. Greece: Petrology, Geochemistry, Geochronology.* Ph.D. thesis, Techn. Univ. Braunschweig, Braunschweig, Germany.

_____ & KREUZER, H. (1990): K–Ar dating of metamorphic

and magmatic rocks from the Xanthi and Drama areas, Greek part of the Rhodope zone. *Eur. J. Mineral.* **2**, 161.

_____ & MPOSKOS, E. (1990): Evolution of the eclogites in the Rhodope zone of northern Greece. *Lithos* **25**, 89-99.

MASSONNE, H.-J. & SCHREYER, W. (1987): Phengite geobarometry based on the limiting assemblage with K-feldspar, phlogopite and quartz. *Contrib. Mineral. Petrol.* **96**, 212-224.

MATTHEWS, A. & SCHLIESTEDT, M. (1984): Evolution of the blueschist and greenschist facies rocks of Sifnos, Cyclades, Greece. *Contrib. Mineral. Petrol.* **88**, 150-163.

MILLER, C. (1977): Chemismus und Phasenpetrologische Untersuchungen der Gesteine aus der Eclogitzone des Tauernfensters, Österreich. *Tschermaks Mineral. Petrogr. Mitt.* **24**, 221-277.

MOTTANA, A., CARSWELL, D.A., CHOPIN, C. & OBERHÄNSLI, R. (1990): Eclogite-facies mineral parageneses. *In* Eclogite Facies Rocks (D.A. Carswell, ed.). Blackie Publications, London, U.K. (14-49).

MPOSKOS, E. (1989a): High-pressure metamorphism in gneisses and pelitic schists in East Rhodope zone (N. Greece). *Mineral. Petrol.* **41**, 337-351.

_____ (1989b): Metamorphic evolution of the lower tectonic unit of east Rhodope (N. Greece), based on the metabasite petrology. *Carpatho-Balkan Geol. Assoc., XIV Congress* **1**, 317-320.

_____ & PERDIKATSIS, V. (1987): High-pressure metamorphism in East Rhodope Massif (Greece). *Fortschr. Mineral.* **65**, *Bh.* **1**, 140.

PATRICK, B.E. & EVANS, B.W. (1989): Metamorphic evolution of the Seward Peninsula blueschist terrane. *J. Petrol.* **30**, 531-555.

POWELL, R. & HOLLAND, T. (1990): Calculated mineral equilibria in the pelite system, KFMASH (K_2O–FeO–MgO–Al_2O_3–SiO_2–H_2O). *Am. Mineral.* **75**, 367-380.

RUBIE, D.C. (1984): A thermal tectonic model for high-pressure metamorphism and deformation in the Sezia zone, Western Alps. *J. Geol.* **92**, 21-36.

SCHLIESTEDT, M. (1986): Eclogite-blueschist relationships as evidenced by mineral equilibria in the high-pressure metabasic rocks of Sifnos (Cycladic Islands), Greece. *J. Petrol.* **27**, 1437-1459.

SPEAR, F.S. & FRANZ, G. (1986): P–T evolution of metasediments from the eclogite zone, south-central Tauern Window, Austria. *Lithos* **19**, 219-234.

THOMPSON, A.B. (1976): Mineral reactions in pelitic rocks. I. Prediction of P–T–X(Fe–Mg) phase relations. *Am. J. Sci.* **276**, 401-424.

_____ & ALGOR, J.R. (1977): Model systems for anatexis of pelitic rocks. I. Theory of melting reactions in the system $KAlO_2$–$NaAlO_2$–Al_2O_3–SiO_2–H_2O. *Contrib. Mineral. Petrol.* **63**, 247-269.

THOMPSON, J.B. (1957): The graphical analysis of mineral assemblages in pelitic schists. *Am. Mineral.* **42**, 842-858.

TRACY, J.R. (1982): Compositional zoning and inclusions in metamorphic minerals. *In* Characterization of Metamorphism Through Mineral Equilibria (J.M. Ferry, ed.). *Rev. Mineral.* **10**, 355-397.

VUICHARD, J.P. & BALLÈVRE, M. (1988): Garnet-chloritoid equilibria in eclogitic pelitic rocks from the Sezia zone (Western Alps): their bearing on phase relations in high pressure metapelites. *J. Metamorph. Geol.* **6**, 135-157.